Computers and Electronics in Agriculture 235 (2025) 110397

Contents lists available at ScienceDirect

Computers and Electronics in Agriculture

journal homepage: www.elsevier.com/locate/compag

Original papers

A novel opto-tactile sensing approach to enhance the handling of soft fruit

Mohamed Adlan Ait Ameur [a,*], Amr M. El-Sayed [a,b,c], Xiu T. Yan [a], Jörn Mehnen [a,*], Anja M. Maier [a]

[a] Design, Manufacturing and Engineering Management, University of Strathclyde, Glasgow, United Kingdom
[b] Mechatronics Engineering Department, Faculty of Engineering, Assiut University, Assiut 71516, Egypt
[c] Department of Mechanical Engineering, Glasgow Caledonian University, Cowcaddens Rd, G4 0BA Glasgow, United Kingdom

ARTICLE INFO

Keywords:
Robotic gripper
Vision-Based Tactile Sensor (VBTS)
Image Processing
Machine Learning
Soft Fruit Handling
Robotic manipulation

ABSTRACT

In agricultural settings, handling of soft fruit is critical to ensuring quality and safety. This study introduces a novel opto-tactile sensing approach designed to enhance the handling and assessment of soft fruit, with a case example of strawberries. Our approach utilises a Robotiq 2F-85 gripper equipped with the DIGIT Vision-Based Tactile Sensor (VBTS) and attached to a Universal Robot UR10e. In contrast to force-based approaches, we introduce a novel purely image-based processing software pipeline for quantifying localised surface deformations in soft fruit. The system integrates fast and explainable image processing techniques applying image differencing, denoising, K-means clustering for unsupervised classification, morphological operations, and connected components analysis (CCA) to quantify surface deformations accurately. A calibration of the image processing pipeline using a rubber ball showed that the system effectively captured and analysed the rubber ball's surface deformations, benefiting from its uniform elasticity and predictable response to compression. As a soft fruit case example, the image processing pipeline was subsequently applied to strawberries, blueberries, and raspberries, demonstrating that the calibration parameters derived from the rubber ball could effectively assess surface deformations in soft fruits. Despite the complex, nonlinear deformation characteristics inherent to strawberries, blueberries, and raspberries, the pipeline exhibited robust performance, capturing and quantifying subtle surface changes. These findings underscore the system's capacity for precise deformation analysis in delicate materials, offering major potential for further refinement and adaptation. This novel approach of proposing and testing an image processing pipeline lays the groundwork for enhancing the handling and assessment of materials with intricate mechanical properties, paving the way for broader applications in sensitive agricultural and industrial settings.

1. Introduction

Global food supply resilience and security is under threat, influenced, for example, by population growth, the need to increase agricultural productivity, the effects of climate change, the complexities of migration, the shift from rural to urban living, and ageing populations (Duckett et al., 2018). As the world population is projected to reach 9.7 billion by 2050, the agricultural sector faces major challenges (United Nations, 2019). Moreover, the agricultural industry is confronted with the challenge of increasing total food demand (Kootstra et al., 2021), necessitating innovative solutions to address these challenges and to ensure the sustainability and security of food supply for future generations. Automated harvesting and grasping of soft fruit have been a bottleneck in agricultural industries, often relying on labour-intensive processes prone to inefficiencies and waste. Cultivation and manufacturing methods are complicated, tedious, and usually specific to each crop (Bechar & Vigneault, 2016). Meeting the current challenges confronting the agriculture and food sectors demands innovative solutions that harness cutting-edge sensing technologies (Zou et al., 2017). As labour shortages intensify due to demographic shifts, there is a critical need for highly automated systems to streamline agricultural processes. This growing demand has fuelled the proliferation of agricultural robots, marking a paradigm shift in farm management practices (Zhang et al., 2020). Integrating robots into agricultural settings aims to facilitate seamless Human-Robot Collaboration (HRC), leveraging the strengths of both farmers and machines to mitigate workforce limitations and optimise agricultural productivity. Robots are viewed as a crucial component of Agriculture 4.0, representing the advancement of

* Corresponding authors.
E-mail addresses: adlan.ait-ameur@strath.ac.uk (M.A. Ait Ameur), jorn.mehnen@strath.ac.uk (J. Mehnen).

https://doi.org/10.1016/j.compag.2025.110397
Received 14 January 2025; Received in revised form 28 March 2025; Accepted 8 April 2025
Available online 16 April 2025
0168-1699/© 2025 The Authors. Published by Elsevier B.V. This is an open access article under the CC BY-NC license (http://creativecommons.org/licenses/by-nc/4.0/).

precision agriculture. This evolution empowers farmers to efficiently utilise precise quantities tailored to specific areas (Benos et al., 2023). According to Vasconez et al. (2019), HRC approaches in agriculture offer potential solutions to intricate challenges, ensuring security, convenience, reduced labour demands, and enhanced productivity throughout various agricultural production and distribution processes.

Humans rely on their sense of touch to manipulate objects and interact with the environment, mainly when visual information is unavailable or limited. This reliance on tactile sensation is a well-documented aspect of human sensory perception (De Maria et al., 2012) and the effectiveness of robotic systems relies on delicately handling items, such as fruits. Conventional robotic grippers available to-date frequently need more sophistication for such tasks, necessitating technological advancements to ensure efficient performance in delicate object manipulation. Incorporating tactile data into robotic systems and other sensing modalities, such as vision, must aim for a cohesive sensory understanding (Mandil et al., 2023). To bridge this disparity, it is imperative to enhance the grasping functionality of robots through sensor-based advancements and their seamless integration into robotic frameworks. Notably, vision-based tactile sensors emerge as promising components among these sensor technologies, offering comprehensive insights into crucial parameters such as fruit firmness, ripeness, and structural integrity. This research proposes a new method for safely handling objects by integrating vision-based tactile sensing capabilities into robotic grippers. We specifically consider the handling of soft fruit as an agricultural case example.

The paper proposes a novel opto-tactile sensing approach that integrates advanced image processing. The system was calibrated using a rubber ball to quantify deformation robustly. Unlike standard pressure-based sensors, which often lack sensitivity for delicate produce, our vision-based tactile method employs image differencing, unsupervised clustering, and morphological operations to capture subtle surface changes, paving the way for more efficient and damage-free fruit handling. This sensor offers detailed visual information crucial for precise grasping strategies, providing real-time feedback on object shape, texture, and orientation. This enables robotic grippers to adjust their grasp dynamically, ensuring safe and effective handling. In this paper, we propose a new software pipeline to assess the impact of soft fruit deformation using a DIGIT® sensor. Our approach employs a tailored image processing and machine learning pipeline that includes denoising, unsupervised K-means clustering, morphological operations, and connected components analysis. As such, the contribution of the current research work is to address the following research question (RQ): How can image processing and machine learning be integrated to quantify deformation in soft fruits like strawberries, raspberries, and blueberries?

The remainder of the paper is structured as follows: Section 2 reviews related work in tactile sensing and robotic fruit handling, establishing the foundational context for this study. Section 3 then outlines the proposed approach and describes the development of a novel tactile data processing system designed explicitly for robotic fruit handling. Section 4 presents the results obtained from controlled experiments using a rubber ball to establish a base line, followed by a case example with strawberries, blueberries, and raspberries to assess the approach's applicability to handle various delicate objects. Section 5 provides a detailed discussion of the findings in relation to the literature, while Section 6 suggests limitations and future directions to refine the system and extend its applicability. Finally, Section 7 summarises the essential findings and their potential impact on advancing tactile sensing and robotic handling technologies for delicate and fragile items.

2. Related work

Tactile sensors have garnered significant attention in recent years due to their versatility and applicability across various industries. Tactile sensors encompass detecting and measuring perpendicular forces on a surface and interpreting gathered information (Girão et al., 2013). These sensors vary in complexity, from basic ones that detect contact location to advanced sensors that measure surface characteristics like texture, firmness, and temperature (Zou et al., 2017). The opto-tactile sensor is one among the various types of tactile sensors, also known as Vision-Based Tactile Sensors (VBTS). Tactile sensing is critically important in the agricultural and food industries for tasks including harvesting, handling, and extracting features from food items (Mandil et al., 2023). VBTS offer high spatial resolution, capturing detailed characteristic data in images for perception (Chen et al., 2022). A tactile sensor based on vision is an innovative optical sensing technology extensively utilised in robotic perception (Zhang et al., 2022). These sensors detect and quantify physical interactions through touch, providing crucial insights into the surrounding environment, thus enhancing robotic systems' performance in perception and manipulation. Their primary function is to identify contact and the force of contact across the fingertip region (Yuan et al., 2017). Tactile sensors improve agricultural operations and efficiency throughout the distribution system, farms, and retail industries by providing accurate force estimation, slip detection, and contact event detection (Fahmy et al., 2024). VBTS are critical for robots to perform precise manipulation tasks by measuring the 3D geometry of contacted objects (Lin et al., 2023a). Erukainure et al. (2022b) proposed a three-probe piezoresistive tactile sensor to estimate kiwifruit stiffness by fusing instantaneous sensor data and machine learning models. The system employed a cantilever beam sensor design, which was validated through finite element simulations and experimental tests on kiwifruit samples.

Tactile sensing can be used in robotic grasping. Recent research has explored innovative approaches to robotic grasping, integrating deep learning, tactile sensing, and soft robotics. In Zhou et al. (2023), fin-ray fingers with integrated tactile sensor arrays were utilised alongside customised perception algorithms to enhance the robot's capability in identifying and handling branch obstructions during harvesting, thereby minimising potential mechanical harm to fruits. Furthermore, Finger-Vision® technology was employed alongside a Baxter robot and a Universal Robot UR3 in a related study (Yamaguchi & Atkeson, 2019) to extract comprehensive object information, including details, distance, position, pose, size, form, and texture, for a diverse range of 30 fruits and vegetables and raw eggs. Meta AI have engineered a high-resolution opto-tactile sensor known as DIGIT®. They have made the sensor's design publicly accessible and are producing it commercially in collaboration with GelSight® tactile sensors (Lambeta et al., 2020). A custom opto-tactile sensor technology, leveraging deep learning, was developed and utilised to assess tactile contact's location, area, and force (Kakani et al., 2021). Another study (Naeini et al., 2019) presented an event-driven neuromorphic camera for monitoring intensity changes within a silicone membrane at the contact point of a tactile sensor. This sensor was designed to estimate contact force and classify various objects during grasping. The study employed Time Delay Neural Network (TDNN) and Gaussian Process (GP) techniques to accurately assess the contact force within a grasp. A soft gripper was introduced by Lin et al. (2023b), combining soft robotics and vision-based tactile sensing technologies to perform grasping, sensing, and sorting activities. Moreover, a non-destructive approach for determining the firmness of cherry tomatoes was proposed (He et al., 2024), which involved monitoring deformation height using a GelSight® sensor and forecasting fluctuations in fruit firmness. Similarly, an opto-tactile sensor incorporating deep learning techniques was introduced by (Ma et al., 2024) for non-destructive measurement of peach firmness, and (Han et al., 2021) proposed a Transformer-based framework for robotic grasping with stiff grippers, which uses both tactile and visual input to ensure secure object grasping.

Girão et al. (2013) introduces a non-destructive method for cherry tomato firmness detection using a GelSight® sensor and a gradient prediction network, validating firmness predictions against a texture analyser. Li et al. (2024) proposed a deep learning-based framework for fruit hardness estimation using the DIGIT tactile sensor, employing a

Capsule Network with a self-attention mechanism to regress hardness values from tactile images. Erukainure et al. (2022a) developed a tactile sensor incorporating a multi-spring configuration to mitigate contact errors arising from surface irregularities and inclination angles in soft tissue stiffness measurements. Finite element analysis and experimental validation confirmed the sensor's robustness in estimating fruit stiffness with high accuracy while reducing measurement variability. Whilst progress has been made in researching and deploying grasping techniques by integrating various sensing modalities and machine learning approaches to enhance the performance and versatility in handling diverse objects in agricultural and industrial settings. However, despite the availability of systems capable of reliably handling fruit without direct force measurement, analysing deformation in fruit-handling scenarios remains crucial, multifaceted, and under-studied to-date. Understanding the deformation patterns during fruit handling enables developing more sophisticated and adaptable systems. By analysing the area and extent of deformation, systems can be tailored to handle various types of fruit, accounting for differences in size, shape, and ripeness. As such, this paper introduces a novel image processing pipeline that leverages tactile data to analyse deformation, aiming to advance robotic manipulation capabilities. This approach enhances the ability to handle a wide range of delicate objects, ensuring gentle and precise manipulation without relying on direct force measurements.

3. Methodology

This section outlines the methodology for analysing tactile sensor data captured during the experiments. The primary goal is to extract precise and meaningful information, such as surface deformation and contact area which are crucial for enhancing robotic manipulation. The methodology uses advanced image processing and machine learning techniques to interpret tactile data accurately. The specific advanced image processing and machine learning techniques were chosen for their speed and explainability. A detailed overview of the image processing pipeline and its calibration process is provided, ensuring the reliability of the extracted data.

3.1. DIGIT a Vision-Based tactile sensor

We integrated DIGIT® (Lambeta et al., 2020), a vision-based tactile sensor, as seen in Fig. 1, with the UR10e robotic arm and Robotiq gripper 2F-85. This sensor boasts several key features, including a reflective elastomer for enhanced tactile sensitivity, a camera utilising the Omnivision OVM7692 with a VGA resolution (640x480) for high-quality image capture and an acrylic window for protection and clarity of vision during operation.

By integrating the DIGIT sensor with the Robotiq 2F-85 gripper, we can capture detailed tactile information through images, enhancing the precision of manipulation tasks. During the calibration process, we operated the DIGIT sensor at a resolution of VGA (640x480) and a frame rate of 30 frames per second (FPS). This resolution was deliberately selected to balance image quality and computational efficiency. Operating at 640x480 provides sufficient detail to discern fine tactile features while maintaining manageable computational overhead, ensuring accurate detection and analysis of contact properties during manipulation tasks. The frame rate of 30 FPS was chosen during calibration to ensure real-time feedback, which is crucial for dynamic manipulation scenarios. By capturing images at this frame rate, DIGIT can provide timely feedback to the robotic system, enabling responsive and adaptive manipulation behaviours.

The Robotiq 2F-85 gripper (Robotiq, 2018) and the Universal Robot UR10e (UR10e, 2023) were selected for our setup. A DIGIT sensor was installed on one side of each finger, while a small soft sponge was affixed to the other side, as depicted in Fig. 2. Adding the sponge to the opposite finger provides a softer, more delicate grip, reducing the risk of damage the gripper's original firm material could cause. The gripper has a maximum opening of 85 mm, and the DIGIT sensor measures 32 mm in length, leaving an average of 53 mm of space available for grasping, ensuring controlled adjustments during manipulation. The grasping force set via the teaching pendant, using the pre-calibrated settings from the manufacturer for the Robotiq 2F-85, was 235 Newtons. This pre-calibrated force ensured secure handling while minimising the risk of damage.

3.2. Overview and calibration of the tactile data processing system

The image processing pipeline proposed and tested in this paper, comprises several key stages designed to refine the data and extract critical features. The process begins with data acquisition from the DIGIT sensor integrated into the Robotiq 2F-85 gripper. Initially, once the object is positioned within the gripper, an image is captured. The gripper's width is then incrementally reduced by 1 mm using the teaching pendant, and a new image is taken at each step. Following this, the initial image is subtracted from each subsequent image captured during the pressing sequence. This subtraction process effectively highlights the changes in surface morphology that occur as the gripper closes. To enhance the visibility of these changes, the resulting difference images are amplified by a factor of 10 within the RGB colour spectrum, making even subtle variations more discernible. After this amplification step, image denoising is performed to improve the clarity of the data. The denoised images are then processed using K-means clustering, an unsupervised machine learning technique, to classify and organise the data based on inherent patterns. Following the clustering, morphological operations are further applied to refine the extracted features' precision and definition. Finally, connected component analysis (CCA) is employed to segment and refine the data, resulting in a structured and detailed understanding of the tactile information. Fig. 3 provides a visual representation of the entire process chain, with the subsequent sections offering a detailed explanation of each step.

We designed an experimental setup to initiate our investigation by

H = 33.5 mm, L = 32 mm, and W = 27 mm.

Fig. 1. DIGIT Vision-Based Tactile Sensor (VBTS).

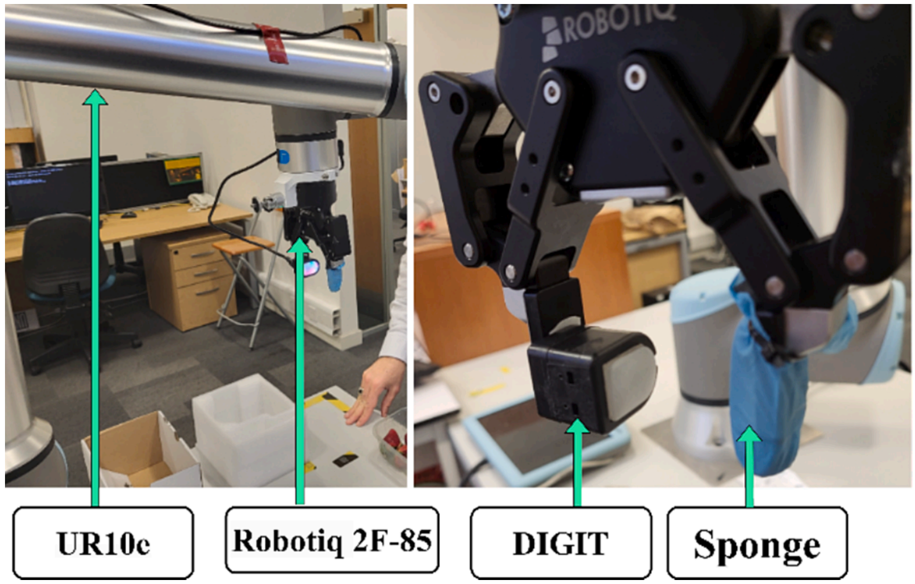

Fig. 2. Robotiq 2F-85 and UR10e setup with DIGIT sensor and sponge integration.

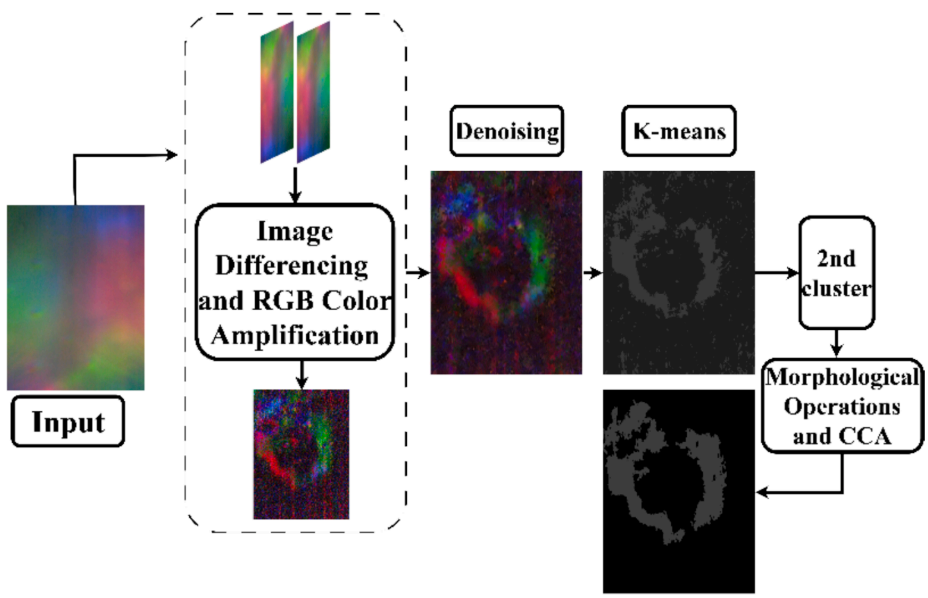

Fig. 3. Proposed tactile data processing system.

integrating the Robotiq 2F-85 gripper with the DIGIT vision-based tactile sensor. The calibration of the data processing pipeline using a rubber ball was set-up as follows: Fig. 4 shows that the rubber ball with a diameter of 24 mm is positioned between the finger of the gripper Robotiq 2F-85 and the DIGIT. This setup allows for precise control over the compression of the rubber ball, ensuring consistent and reproducible conditions for data collection. The DIGIT sensor captures detailed tactile images of the rubber ball's surface throughout the compression process. This setup is critical, as it provides the foundational data needed to analyse the sensor's performance in detecting subtle changes in surface morphology. This calibration experiment using a black rubber ball also helps, for the first time, with assessing the sensitivity of the DIGIT sensor in detecting small changes when compressing objects with predictable properties.

The rubber ball was compressed between the gripper's fingers, with the gripper width reduced in 1 mm increments using the teaching pendant from an initial width of 46 mm to a final width of 33 mm, resulting in 14 distinct images, as seen in Fig. 5. These images allowed us to adjust the workflow parameters, ensuring the tactile data accurately reflects the physical deformations observed during compression. The captured images were analysed following data capture to determine the optimal parameters for the processing pipeline's denoising, feature extraction, and classification steps.

These images, recorded at a resolution of 640x480 pixels and a frame rate of 30 frames per second, are integral to our analysis. They allow us to trace the progression of deformation in fine detail, offering a sequential view of how the rubber ball's surface characteristics evolve under varying pressure levels. This data acquisition stage is crucial for generating a comprehensive dataset that supports our subsequent analytical efforts. To fully understand the changes in surface morphology, it is essential to analyse the RGB histogram channels in Fig. 6, which will provide deeper insights into the material's response to applied pressure.

The red channel intensity histograms shown in Fig. 6 reveal

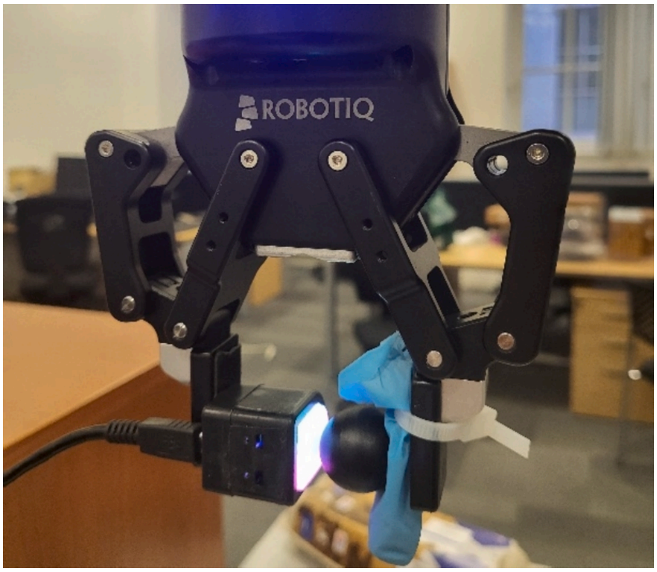

Fig. 4. Calibration setup of DIGIT using the rubber ball.

significant shifts and broadening as the rubber ball is compressed. Initially, the red channel displays distinct peaks, which become less pronounced with increased pressure, indicating surface texture and reflectivity changes. This broadening and the diffusion of intensity peaks suggest that the contact area between the sensor and the ball expands, reflecting the ball's deformation under pressure. The red channel's ability to capture these changes highlights its effectiveness in monitoring surface characteristics during compression, providing critical insights into the material's response to applied force.

The green channel intensity histograms in Fig. 7 show a noticeable shift and broadening as the rubber ball is compressed, starting with a sharp peak in the initial image that becomes more diffuse. This broadening indicates an expanding contact area and changes in surface texture as pressure is applied. The green channel's sensitivity to these variations highlights its effectiveness in capturing subtle surface deformations during the tactile interaction, making it crucial for analysing the sensor's performance in this experiment.

The blue channel intensity histograms in Fig. 8 show a more moderate shift than the red and green channels as the rubber ball is compressed. Initially, the blue channel exhibits a sharp peak, which broadens slightly as pressure increases, reflecting a consistent but less pronounced change in surface texture and contact area. This moderate broadening suggests that the blue channel is less sensitive to surface texture variations but effectively captures the overall expansion of the contact area. The stability in the blue channel's response complements the more pronounced changes observed in the other channels, providing a balanced view of the surface deformation process.

To elucidate the surface deformations captured by the DIGIT sensor during the rubber ball's compression, we employed a technique that subtracted the initial image from subsequent ones obtained during the pressing sequence. This subtraction process effectively highlights the changes in surface morphology that occur as the gripper incrementally reduces its width. To further enhance the visibility of these changes, each resulting difference image was amplified by a factor of 10 within the RGB colour spectrum, making even subtle surface variations more discernible.

As shown in Fig. 9, the amplified difference images illustrate the gradual deformation of the rubber ball's surface as the gripper closes. The first image represents the ball's initial grasp (image 1), while the final image shows the ball at its most compressed state (image 13). The

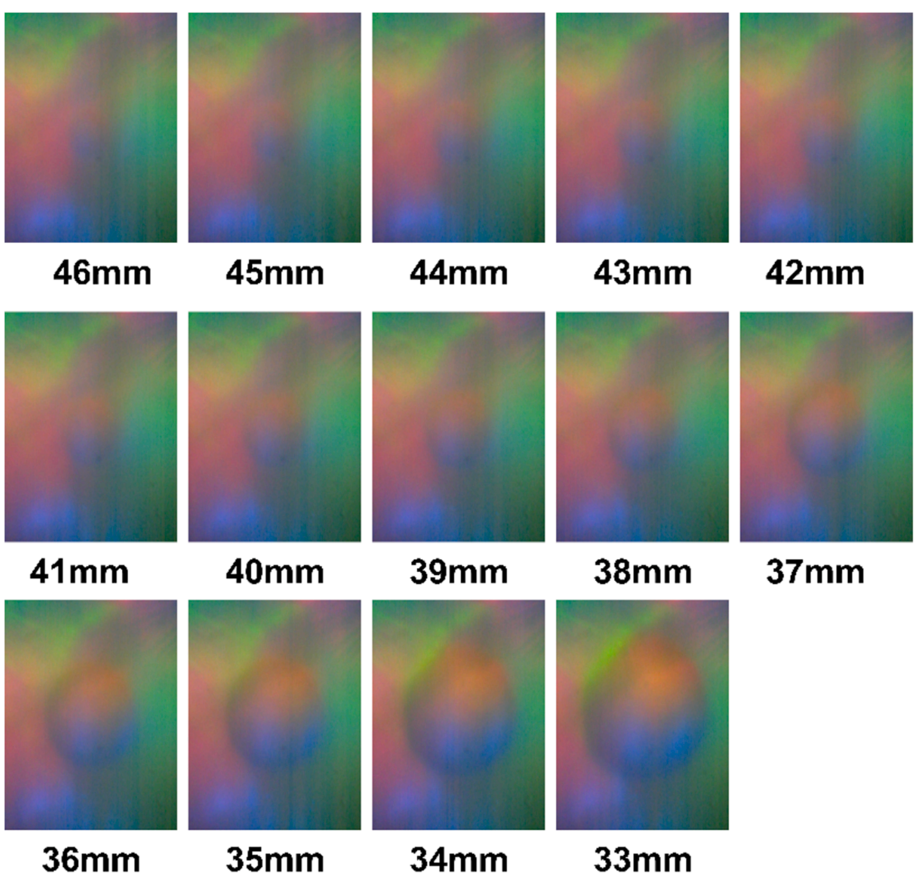

Fig. 5. Images captured by DIGIT as a result of calibration using the rubber ball.

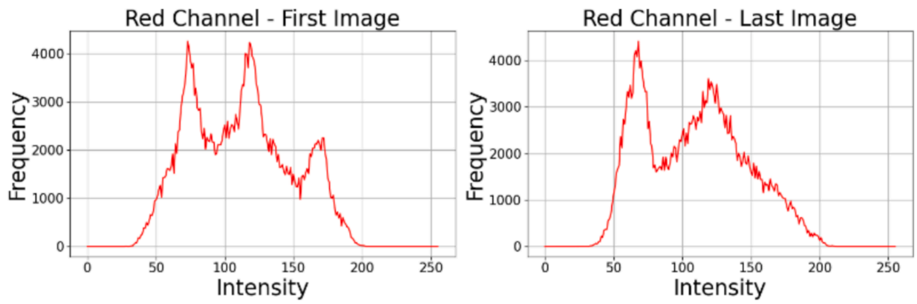

Fig. 6. Comparing the red channel images of the rubber ball from the first and last raw images.

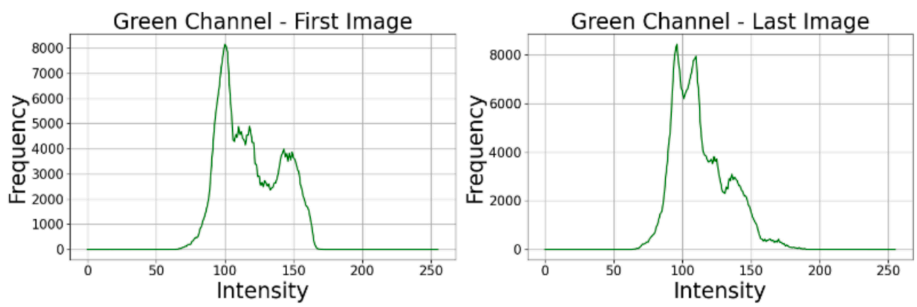

Fig. 7. Comparing the green channel images of the rubber ball from the first and last raw images.

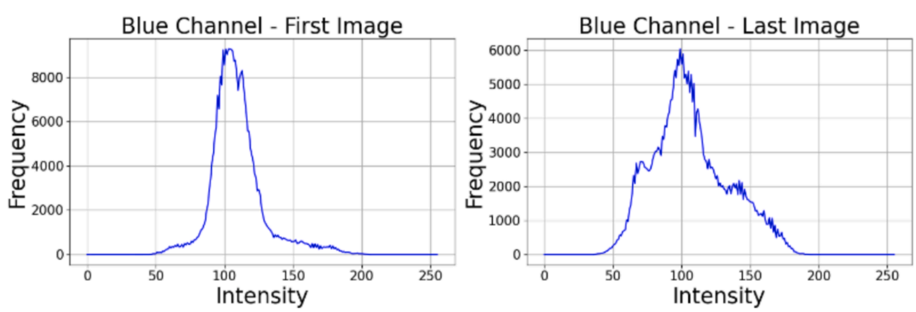

Fig. 8. Comparing the green channel images of the rubber ball from the first and last images.

sequence of images clearly shows the expansion of the contact area between the gripper and the rubber ball and the corresponding changes in surface texture and reflectivity. This method successfully visualises the gradual morphological changes during compression, representing the deformation process.

In the difference images, the colours represent changes in pixel intensities across the RGB channels as the rubber ball is compressed. The red area indicates increased red channel intensity, suggesting surface texture or angle changes that result in more red-light reflection. Green areas highlight increases in green channel intensity, likely corresponding to surface stretching or changes in the contact area with the gripper. Blue areas show where blue channel intensity has increased, potentially indicating surface alterations such as minor compressions or shadow formation. Mixed colours like cyan and magenta suggest simultaneous changes in multiple channels, pointing to complex deformations. Darker regions indicate minimal changes in all channels, signifying areas where the rubber ball's surface experienced little to no deformation or compression. These colour variations provide a visual map of the rubber ball's surface deformation, offering insights into the material's response under pressure.

Following this visual analysis of the images, the next phase involves processing these images through a series of advanced techniques to extract further meaningful data. The pipeline begins with the denoising of the images to reduce noise and enhance clarity, ensuring that the subsequent steps operate on the most accurate data possible. This is followed by applying K-means clustering, an unsupervised machine learning technique, to classify and group the data based on pixel intensity and structural similarity. After clustering, morphological operations are applied to refine the detected features, smoothing and enhancing the segmented regions to better reflect the deformations. Finally, connected components analysis (CCA) identifies and labels distinct regions within the images, isolating significant features related to the rubber ball's surface deformation. This refined segmentation ensures that the analysis captures the true extent of the deformation with high precision. This comprehensive approach allows us to move beyond simple visual inspection and into a deeper, more quantitative analysis of the tactile data, offering valuable insights into the rubber ball's material properties and the DIGIT sensor's performance in capturing fine-grained surface details during robotic manipulation tasks.

- Denoising

A denoising procedure using Non-Local Means Denoising was employed to enhance the fidelity of the tactile sensor data captured (Buades et al., 2011). It aims to estimate the actual pixel value of an image by averaging intensities of similar pixels in a local neighbourhood. This averaging process is weighted based on the similarity between neighbourhoods centred at the current pixel and all other pixels in

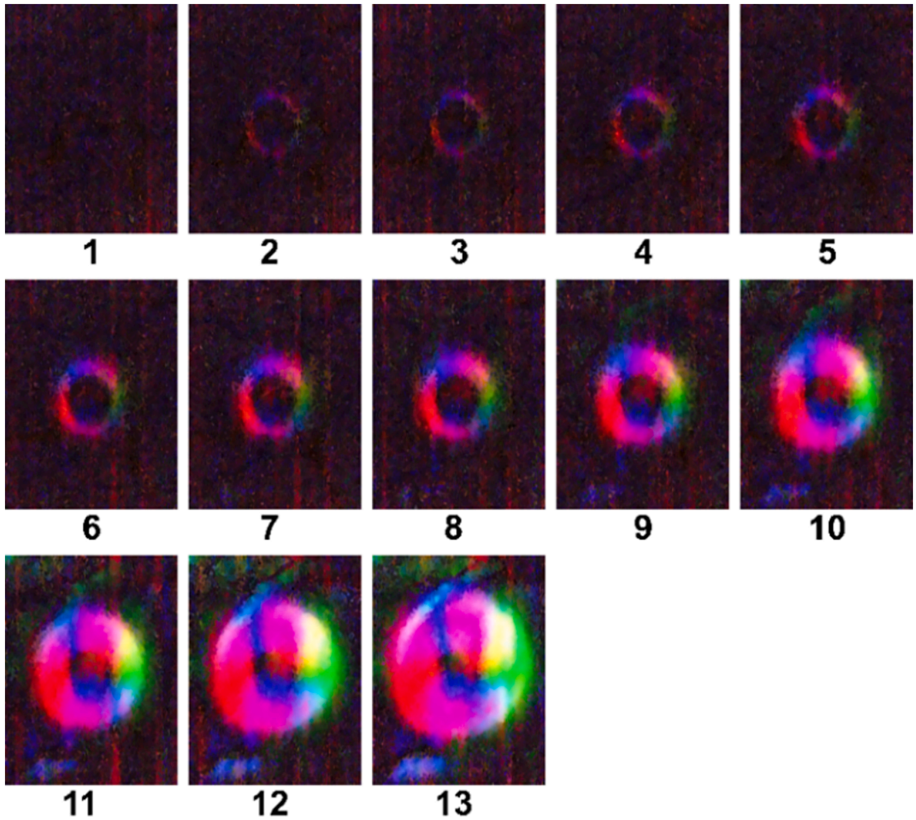

Fig. 9. Difference image sequence represents the ball's initial grasp to the ball at its most compressed state highlighting surface deformation in rubber ball compression.

the image. This can be divided into four steps.

Step 1: Euclidean Distance Calculation

Given an input image I represented as a 3D matrix where Ix,y,c represents the intensity of colour channel c at pixel (x,y), we define the Euclidean distance $d(B(p), B(q))$ between image patches centred at points p and q, where $B(p)$, $B(q)$ represent an image patch centred at point p and q. This distance measures the dissimilarity between the neighbourhoods centred at points p and q.

Step 2: Weighted Averaging

A decreasing function f (Buades et al., 2011) is applied to this distance. This function assigns higher weights to more similar neighbourhoods (i.e., have smaller distances). The weighted averaging process can be represented in Eq. (1):

$$O(p) = \frac{1}{C(p)} \int f(d(B(p), B(q)) u(q) dq \tag{1}$$

The statement refers to the calculation of the Euclidean distance $d(B(p), B(q))$ between image patches centred at points p and q where $O(p)$ is the denoised pixel value at location p, $C(p)$ is a normalising factor, $u(q)$ represents the intensity of the pixel at location q, and the integral is taken over all pixels in the image.

Step 3: Normalization Factor

The normalisation factor (p) ensures that the weighted averaging process is appropriately scaled and that pixels with more prominent neighbourhoods (typically including more similar pixels) do not dominate the averaging process.

Step 4: Denoising Parameters

The OpenCV library implementation was utilised in our case, with the parameters set as shown in Table 1. Determining the parameters for subsequent steps involved a trial-and-error process with the rubber ball. These parameters included a filter strength of 20, window sizes for template matching set to 20, a search space of 7, and a colour-specific filtering strength of 21.

For image processing, three standard metrics are used to quantify the quality of images are PSNR (Peak Signal-to-Noise Ratio), MSE (Mean Squared Error), and SSIM (Structural Similarity Index Measure). PSNR measures the similarity between two images by comparing their pixel values, while MSE calculates the average squared difference between corresponding pixels. SSIM, on the other hand, considers structural information to assess perceptual similarity. These metrics are valuable for tasks like image denoising, compression, and enhancement, aiding in objectively evaluating and comparing image processing algorithms. This denoising step enables more accurate analysis and decision-making for our subsequent image segmentation using K-means.

- Unsupervised Machine Learning (K-means)

K-means clustering is an unsupervised machine learning approach that divides data into discrete groups, or clusters, based on similarity

Table 1
Denoising parameters.

Parameters	Number
Filter Strength(h)	20
Window sizes for template matching (templateWindowSize)	20
Search space (search window size)	7
color-specific filtering strength (hForColorComponents)	21

(Kodinariya & Makwana, 2013). It is widely used in various applications, including robotics, for object identification, motion planning, and environment modelling tasks. K-means clustering divides a dataset into k groups and assigns each data point to the cluster with the closest mean. Our study used a cluster number of $k = 2$. This choice entails partitioning the data into two clusters by iteratively updating cluster centres to minimise the total within-cluster variance. The algorithm continues this process until convergence, ultimately yielding two distinct clusters that effectively capture the underlying structure of the image. Convergence criteria are met, such as when the cluster centres no longer change significantly or after a fixed number of iterations.

- Morphological operation and connected components analysis

Morphological operations (Comer & Delp III, 1999) are fundamental techniques in image processing that analyse and alter the shape and structure of objects within an image. These operations, including Dilation, Erosion, Opening, and Closing, rely on the interaction between an input image and a kernel, also known as a structural element. They find applications in noise reduction, edge detection, and object segmentation tasks. In our method, two critical morphological operations, Closing and Opening, are employed to remove noise and enhance the quality of grayscale image segmentation. Specifically, these operations are used to eliminate minor, noisy artifacts, thereby improving the overall accuracy and quality of the segmentation process. We conducted trial-and-error experiments to optimise these operations using a rubber ball as the test object. These experiments determined that a 3x3 square kernel was the most effective for our purposes. This kernel size balances removing minor noisy artifacts and preserving relevant details, ensuring consistent and reproducible results in our image processing pipeline. Connected Components Analysis (CCA) identifies, and labels connected regions within the grayscale image (Datacarpentry, 2024).

Following an Opening operation to remove small noise regions, the connected components are analysed, and elements with an area below a specified threshold (in our case, 5000 pixels) are filtered out. The choice of this threshold value was determined through iterative experimentation. It was observed that noise regions typically amounted to approximately 5000 pixels. This filtering process ensures that only significant regions corresponding to the objects of interest (Ko & Nam, 2006) are retained in the final segmented image, facilitating the identification and subsequent removal of noise regions below the specified threshold.

With the calibration of the image processing pipeline using the rubber ball completed, we have now established a robust foundation for applying this process chain to more complex and delicate tasks, such as handling of soft fruit. The next step involves using the calibrated system to analyse the rubber ball and strawberries' surface deformations during robotic manipulation. This transition from the controlled calibration environment of the rubber ball to the variable textures and shapes of strawberries will allow us to test the pipeline's adaptability and accuracy in real-world scenarios. The results from these experiments will provide critical insights into the approach's effectiveness and potential applications in the precise handling of soft fruits.

4. Results

4.1. Controlled deformation analysis for rubber ball experiments

Denoising: our approach to enhancing the fidelity of tactile sensor data involved employing a denoising procedure utilising the non-local means denoising (Buades et al., 2011) technique. This method estimates the pixel values of an image by averaging intensities of similar pixels within a local neighbourhood. The size of this neighbourhood is a critical parameter in the denoising process, impacting both the effectiveness and computational efficiency of the algorithm. In our implementation, we opted for a relatively large neighbourhood size, achieved through parameters such as the template window size of 20 and the search window size of 7. This choice enables the algorithm to consider a broad spatial extent when removing noise, facilitating the capture of intricate patterns and variations within the image. The results of this denoising process of the rubber ball can be observed in Fig. 10.

The metrics presented provide a detailed evaluation of the denoising quality achieved in the image processing procedure, as shown in Table 2. A PSNR value of 26.42 dB signifies that the denoised image retains a moderate level of quality relative to the noisy counterpart, indicating some loss due to residual noise. The MSE value of 148.19 reflects a noticeable disparity between the two images, underscoring the remaining noise artifacts that were not eliminated during the denoising process. The SSIM value 0.55 also suggests a moderate structural similarity between the noisy and denoised images. While the images share some standard structural features, they are not identical, and the SSIM value reflects the balance between noise reduction and the preservation of essential image details. This analysis highlights the trade-offs inherent in the denoising process, where the objective is to minimise noise without compromising the integrity of critical image information.

K-means: in our study, we chose to set the number of clusters, k, to 2 in the K-means algorithm, a decision made to capture the underlying structure of the image effectively. This choice resulted in the data being partitioned into two clusters: the first representing the background and the second representing the segmented area with noise, as illustrated in Fig. 11. Specifically, the background is depicted by the first cluster, while the second cluster corresponds to the segmented area with noise. The segmentation process enabled us to identify the deformation area of the rubber ball, which appears as the segmented region amidst the background. It is important to note that small noises were also captured around the image during this processing, a detail that will be addressed in subsequent steps of our analysis.

Morphological and Connected Component Analysis: in the methodology, we detailed the pivotal role of morphological operations, specifically Closing and Opening, in enhancing the quality of grayscale image segmentation. After performing a Closing and Opening to remove small noise regions, components with areas below the specified threshold of 5000 pixels were filtered out, facilitating the extraction of meaningful information from the segmented image. The results of these operations can be observed in Fig. 12, illustrating the effectiveness of the morphological operations and CCA in enhancing image segmentation and object identification. The implemented framework demonstrated successful segmentation on the rubber ball, effectively capturing the areas deformed by the DIGIT sensor.

Fig. 13 presents the successful segmentation of the rubber ball under varying gripper widths, illustrating the effectiveness of the optical tactile sensing approach. The images are structured in three distinct rows: the top row represents the image differences, capturing variations in optical feedback due to mechanical deformation; the middle row showcases denoised images, where noise reduction techniques enhance the clarity of the contact regions; and the bottom row displays the segmented images, isolating the deformed area of the rubber ball. As the gripper width decreases from 42 mm to 35 mm, the segmented area progressively increases, reflecting the compression of the rubber ball and the corresponding expansion of its exposed surface. This trend highlights the pipeline's ability to detect and quantify changes in

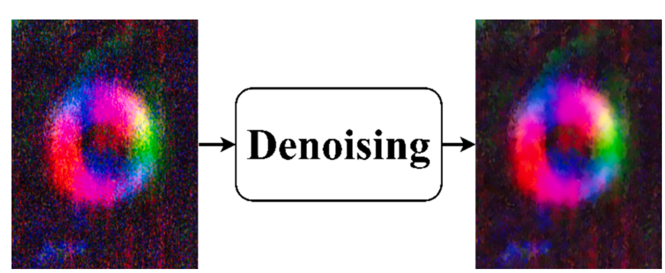

Fig. 10. Image denoising comparison.

Table 2
Image quality metrics comparison.

Metrics	Value
PSNR (dB)	26.422
MSE	148.197
SSIM	0.550

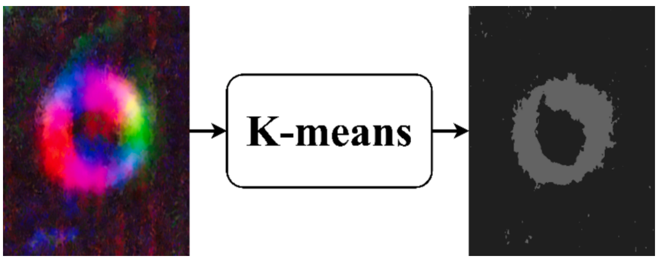

Fig. 11. K-means segmentation.

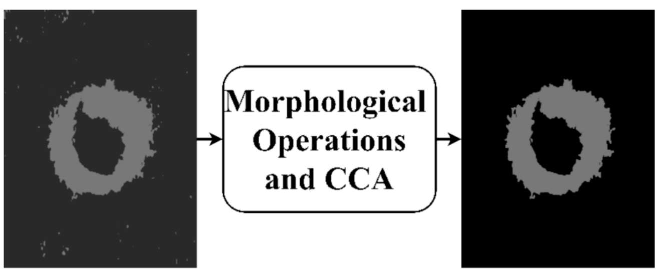

Fig. 12. Morphological operation and connected component analysis (CCA).

deformation effectively, providing valuable insights into the interaction dynamics between the gripper and soft objects. These findings demonstrate the segmentation method's effectiveness in analysing the rubber ball's mechanical responses.

Fig. 14 illustrates the correlation between gripper width differences and the segmented pixel area for a rubber ball using optical tactile sensing. The x-axis represents the gripper width difference in millimeters, while the y-axis indicates the segmented pixel area derived from image processing techniques. Distinctly colored dashed lines denote different test runs (Test 1 through Test 14), demonstrating consistent trends where an increase in gripper width difference results in corresponding variations in segmented pixel area. This correlation highlights the capability of the optical sensing method to effectively quantify deformation, thereby validating its potential application in assessing the quality of soft fruits.

A general upward trend in pixel area is observed with increasing gripper width differences, suggesting that as the rubber ball undergoes deformation, its surface exposure captured by the sensor also increases. These findings confirm that compressing the rubber results in a larger segmented area, demonstrating the effectiveness of the tactile sensing approach.

4.2. Soft fruit picking: Configuring universal robot with Robotiq gripper

To test the image processing approach, we selected thirty strawberries (S1 to S30), each varying in size and shape, as a case study of soft fruit. Using a Robotiq gripper calibrated according to the instruction manual, we captured detailed tactile information with the DIGIT sensor while manipulating each strawberry. The variety in size and shape, as illustrated in Fig. 15, visually represents the strawberries used in the study, providing a comprehensive dataset to evaluate the system's effectiveness in capturing surface deformations.

Table 3 outlines each strawberry's attributes. We focused on how the DIGIT sensor recorded surface changes during compression, offering valuable insights into the strawberries' tactile characteristics under varying conditions.

With our setup finalised, involving the initialisation of the Robotiq gripper through the teaching pendant of the UR10e and DIGIT sensor, as depicted in Fig. 16, we proceeded with the initial grasping action of a strawberry. We successfully executed the grasping action by gradually adjusting the gripper width using the teaching pendant until the strawberry was securely grasped. Following this, the initial image capture was performed using the DIGIT sensor, adhering to the specifications outlined in the previous section. Specifically, we opted for VGA

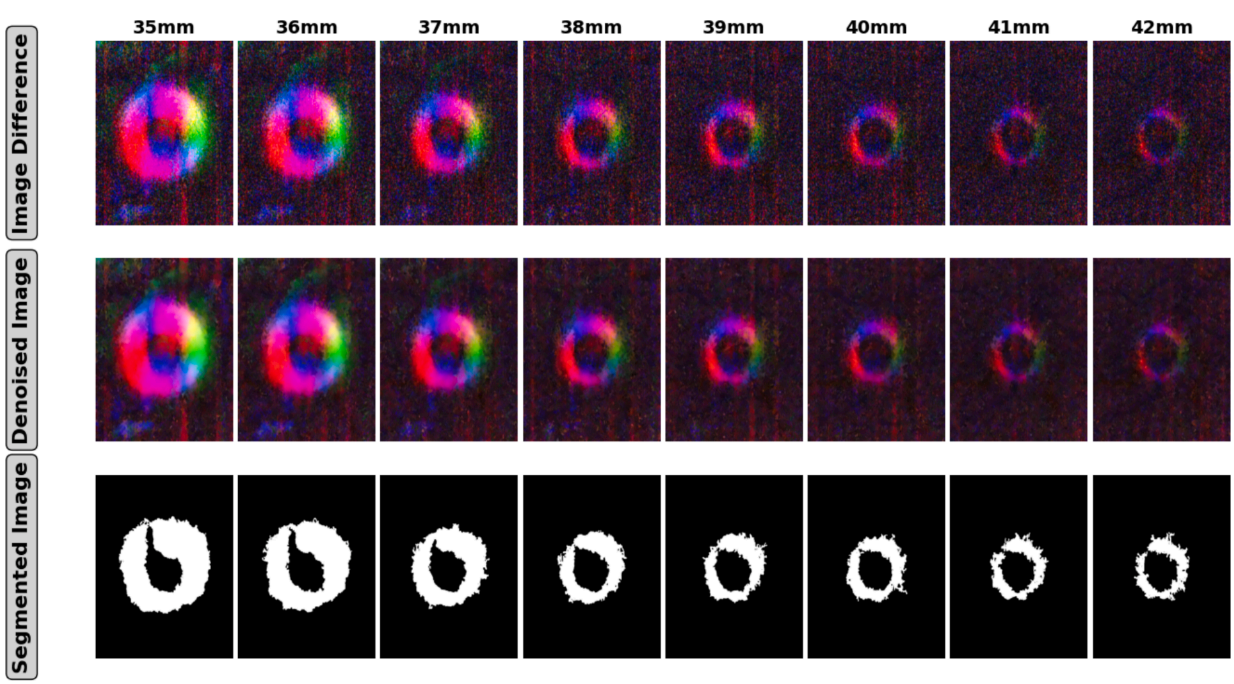

Fig. 13. Optical tactile sensing analysis of rubber ball: Image processing workflow for rubber ball from 42 mm to 35 mm gripper width differences.

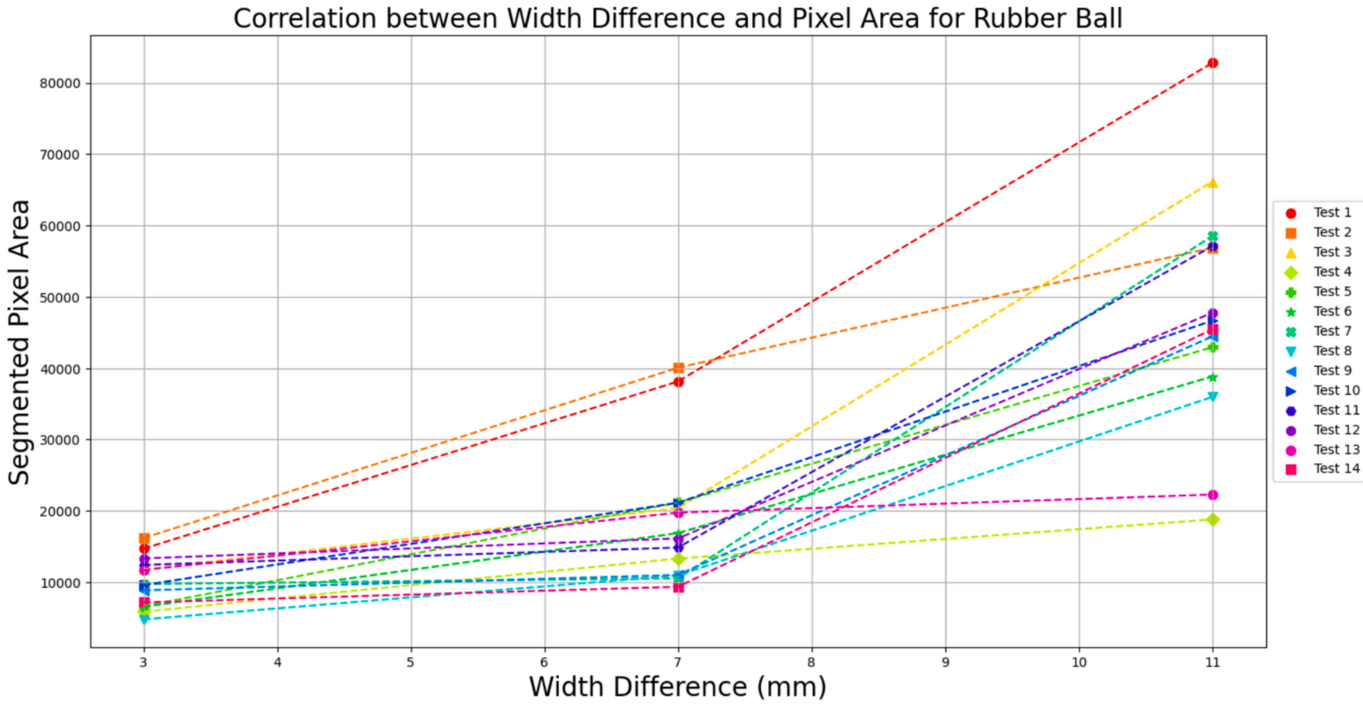

Fig. 14. Correlation between gripper width variation and segmented pixel area in optical tactile sensing of rubber ball.

Fig. 15. Strawberry samples.

Table 3
Strawberries characteristics.

Strawberries	S1	S2	S3	S4	S5	S6	S7	S8	S9	S10	S11	S12	S13	S14	S15	Average
Weight(g)	55.4	32.4	20.8	21.7	23.0	20.2	23.2	17.9	25.3	30.9	24.3	29.1	24.5	30.6	22.4	26.78
Length(mm)	65.51	41.50	43.85	44.69	46.41	42.71	40.17	46.03	43.18	49.85	52.88	57.07	55.30	46.82	39.58	47.70
Width(mm)	48.31	43.03	31.91	34.11	31.46	35.32	36.58	29.69	38.08	38.82	33.56	37.84	29.45	39.10	36.82	36.27
Strawberries	**S16**	**S17**	**S18**	**S19**	**S20**	**S21**	**S22**	**S23**	**S24**	**S25**	**S26**	**S27**	**S28**	**S29**	**S30**	**Average**
Weight(g)	22.5	33.2	18.9	21.8	26.4	20.7	10.2	11.8	28.1	18.5	30.0	32.0	35.0	8.9	16.4	22.29
Length(mm)	49.32	50.44	39.62	35.30	50.35	46.19	29.85	36.92	47.44	42.05	49.38	49.71	54.00	28.24	37.71	43.10
Width(mm)	33.08	40.09	35.55	36.18	37.10	33.34	25.47	25.14	39.09	31.30	42.46	38.50	27.11	31.24	36.42	34.138

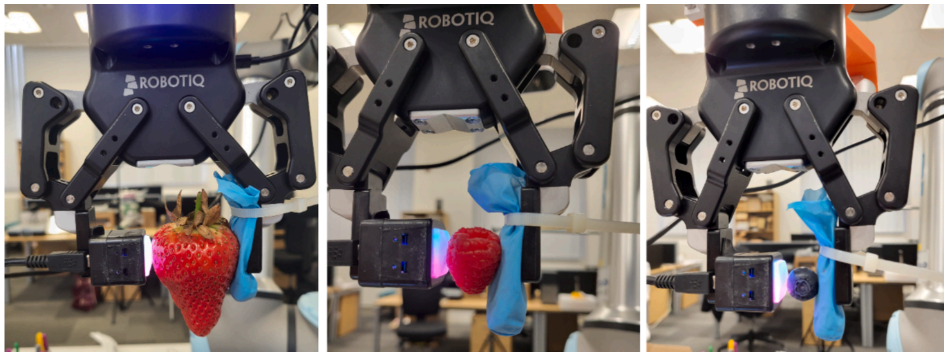

Fig. 16. Initial strawberry (left), raspberry (middle), and blueberry (right) grasping experiment.

quality, capturing at a rate of 30 frames per second, with a resolution of 640 pixels in width and 480 pixels in height.

To further validate the image processing pipeline approach, we conducted the same experimental procedure on thirty raspberries (R1 to R30), each exhibiting variations in size and shape. The calibrated Robotiq gripper was used to manipulate the raspberries while the DIGIT sensor captured tactile responses. The dataset enables an in-depth analysis of surface deformations in soft, delicate fruits. The distinct structural characteristics of the raspberries, as illustrated in Fig. 17, provide a comprehensive dataset to assess the system's effectiveness in capturing surface deformations in soft and delicate fruit.

Table 4. outlines the attributes of the selected raspberries, including weight, length, and width.

Following the same methodology, we initialised the Robotiq gripper via the UR10e teaching pendant and adjusted the grasping width to securely hold each raspberry without excessive deformation, as seen in Fig. 16. The DIGIT sensor recorded surface changes during the grasping process, allowing for the analysis of tactile responses under varying conditions.

Additionally, the experiment was extended to thirty blueberries B1 to B30, characterized by their compact and firm structure Fig. 18. This dataset provides a contrasting case for evaluating the system's ability to detect deformations in small, round fruits. Each blueberry was manipulated using the calibrated Robotiq gripper while the DIGIT sensor recorded detailed tactile information.

Table 5 Blueberries characteristics.

The Robotiq gripper was initialised via the UR10e teaching pendant, and the grasping width was carefully adjusted to ensure a secure hold while minimising excessive force, as depicted in Fig. 16.

With the initial grasping and image capture completed, we now have a comprehensive dataset that will be used to assess our image processing pipeline's effectiveness in analysing blueberries, raspberries, and strawberries' surface deformations. This dataset includes 30 samples per fruit type, with 20 opto-tactile images captured per sample during compression. This structured dataset comprehensively evaluates surface deformations across different fruit textures. Following the careful calibration of the pipeline using the rubber ball, the controlled capture of high-resolution images allows us to apply our system to this delicate soft fruit confidently. In the next section, we are presenting the results of our analysis, discussing the system's performance and the insights gained from applying it to strawberries, blueberries, and raspberries as a case example. This will thoroughly evaluate the system's capability to handle and analyse soft fruits in a robotic manipulation context.

4.3. *Assessment of soft fruit deformation*

4.3.1. *Strawberry case example*

Building on the initial analysis performed on the rubber ball, we extended the application of our image-processing framework to the strawberry, a more complex and irregular object. The methodology, which proved effective in segmenting and analysing the deformation areas of the rubber ball, was applied to the strawberry to assess its efficacy in a more challenging, real-world context. This section details the results of applying the same steps, denoising, K-means clustering, morphological operations, and connected components analysis (CCA), to the strawberry. The aim was to accurately segment the deformed regions caused by the DIGIT sensor and evaluate the segmentation process's robustness when applied to a natural, textured surface. The following results illustrate the effectiveness of this approach in isolating and analysing the deformation patterns on the strawberry.

As outlined in the methodology, the gripper's setup was followed by capturing images throughout the pressing sequence. The process began with an initial image of the strawberry at the onset of grasping. Subsequently, the width of the gripper was decreased by 1 mm at each step,

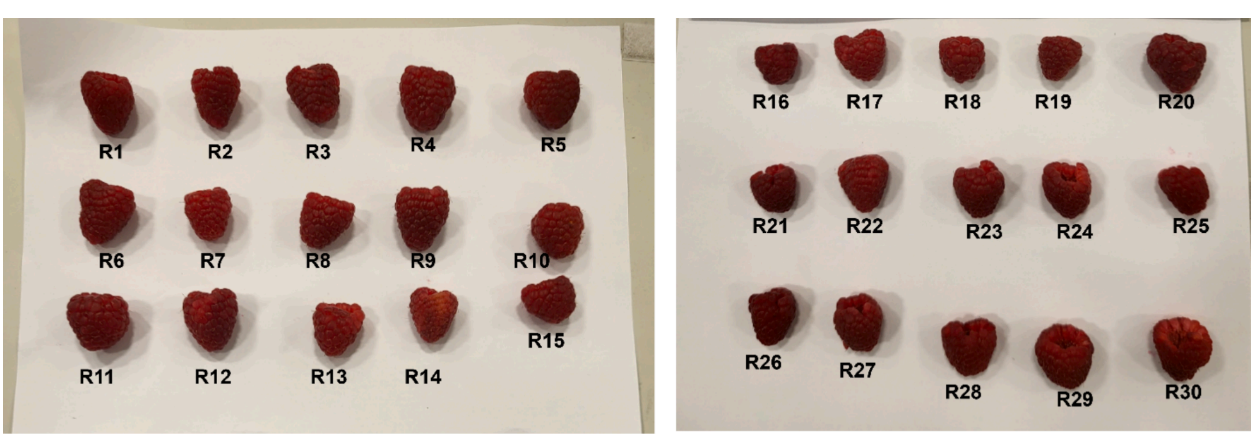

Fig. 17. Raspberry samples.

Table 4
Raspberries characteristics.

Raspberries	R1	R2	R3	R4	R5	R6	R7	R8	R9	R10	R11	R12	R13	R14	R15	Average
Weight(g)	6.9	5.6	5.7	7.2	6.4	6.4	4.8	5.5	6.7	5.2	7.5	6.5	5.0	3.9	4.0	5.8
Length(mm)	27.08	26.14	23.08	26.53	24.87	26.81	23.35	23.97	27.24	22.48	25.71	24.70	21.48	23.75	17.56	24.31
Width(mm)	21.73	21.72	23.43	26.03	24.26	24.46	22.06	21.01	24.41	23.01	25.46	23.01	21.57	21.00	22.27	23.02
Raspberries	**R16**	**R17**	**R18**	**R19**	**R20**	**R21**	**R22**	**R23**	**R24**	**R25**	**R26**	**R27**	**R28**	**R29**	**R30**	**Average**
Weight(g)	3.8	5.6	4.7	4.0	8.2	4.5	6.2	6.7	6.2	4.4	4.5	5.5	5.4	6.9	6.2	5.5
Length(mm)	18.51	22.85	21.15	22.20	26.58	20.95	26.72	23.56	25.50	22.47	22.41	23.82	21.44	26.95	25.61	23.38
Width(mm)	19.18	23.63	21.90	19.73	28.09	21.04	21.80	24.40	22.25	19.60	20.73	21.76	22.12	26.58	23.15	22.39

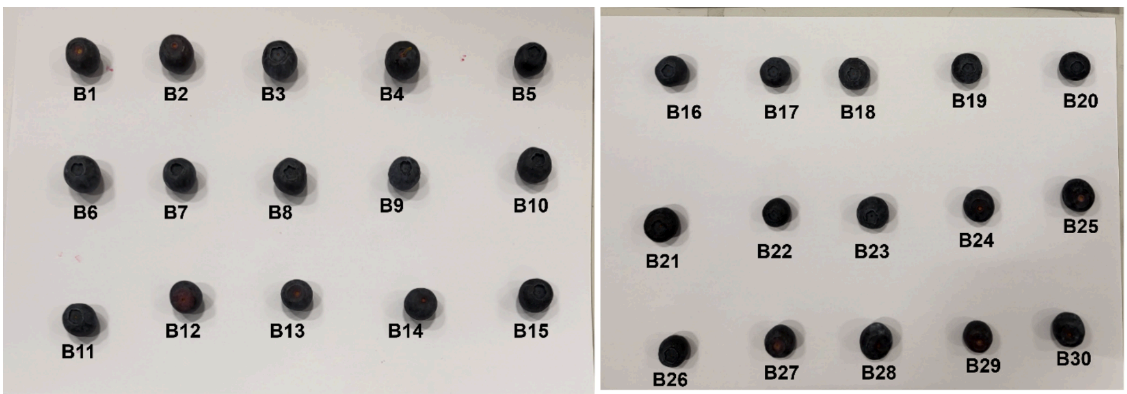

Fig. 18. Blueberry samples.

Table 5
Presents the measured attributes of each blueberry, including weight, length, and width.

Blueberries	B1	B2	B3	B4	B5	B6	B7	B8	B9	B10	B11	B12	B13	B14	B15	Average
Weight(g)	2.4	2.1	2.1	2.3	1.7	2.4	1.9	2.2	1.7	1.9	1.8	1.5	1.6	1.7	2.1	1.9
Length(mm)	17.48	16.48	16.65	17.18	14.84	17.00	15.78	16.65	15.07	15.88	15.60	13.89	15.16	14.53	15.00	15.81
Width(mm)	16.76	15.65	16.77	17.02	14.89	16.00	15.28	15.90	15.30	14.96	15.30	14.53	14.63	14.77	15.44	15.81
Blueberries	**B16**	**B17**	**B18**	**B19**	**B20**	**B21**	**B22**	**B23**	**B24**	**B25**	**B26**	**B27**	**B28**	**B29**	**B30**	**Average**
Weight(g)	2.1	2.2	2.3	2.1	1.9	2.2	1.4	2.1	1.9	2.0	1.5	1.6	2.3	1.5	2.1	1.9
Length(mm)	16.77	14.72	16.44	15.70	15.73	16.38	14.55	16.54	16.29	17.24	15.08	16.00	17.50	15.45	16.48	16.05
Width(mm)	15.88	15.38	16.86	15.79	16.10	17.69	14.55	16.44	16.34	17.39	15.05	15.75	16.01	15.00	16.52	16.05

with an image captured after each adjustment until the strawberry became partially deformed, as shown in Fig. 19. The pressing process was halted when the strawberry reached a point where it began releasing liquid, indicating that it had undergone significant deformation.

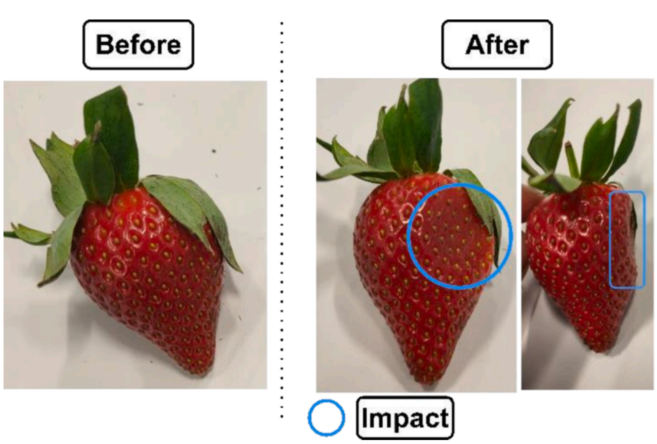

Fig. 19. Comparison of strawberry before and after compression by Robotiq gripper with DIGIT sensor.

Initially, each strawberry had a different gripper width, reflecting their varying sizes. This final width varied due to the strawberries' differing textures and resistance levels. The difference between the initial and final gripper widths was then calculated to measure each strawberry's compression extent. This variation in compression highlights the influence of both the initial size and the inherent texture of each strawberry on the squashing process. Fig. 20 displays a series of 20 images captured by DIGIT, illustrating the progression of strawberry one being pressed at each incremental step of gripper width reduction.

After capturing the images using the DIGIT sensor, the process chain was applied to the same process previously utilised with the rubber ball. The segmentation process is initiated with denoising to reduce noise, followed by K-means clustering to group pixels, morphological operations to refine shapes, and CCA to identify distinct regions.

Fig. 21 presents a three-stage image processing workflow for detecting strawberry variations, focusing on image difference, denoising, and segmentation. The columns represent different strawberries (Strawberry 1 to Strawberry 10), while the rows correspond to the processing stages: (1) Image Difference, (2) Denoised Image, and (3) Segmented Image. In the first row, the Image Difference captures variations between reference and target images, highlighting structural changes across different strawberry samples. The presence of noise and

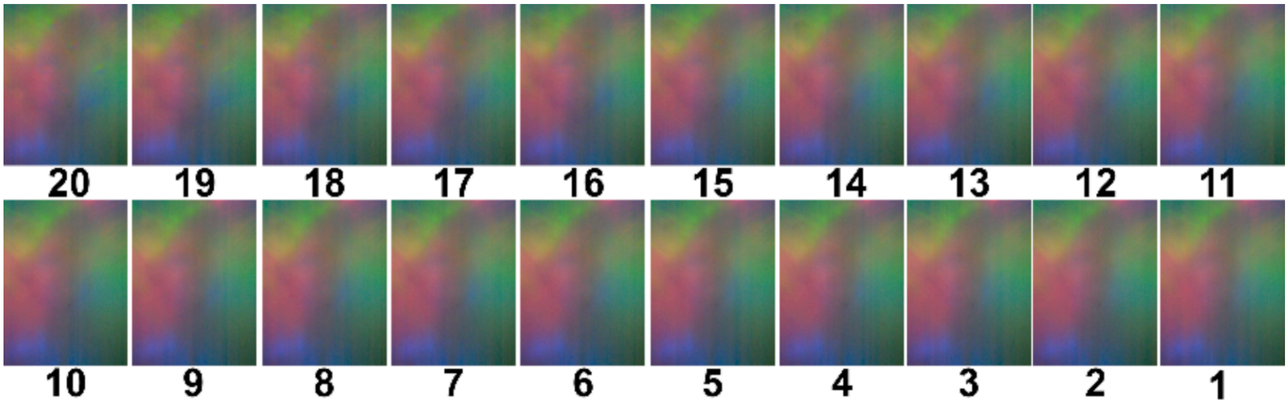

Fig. 20. Images taken by DIGIT of strawberry S1.

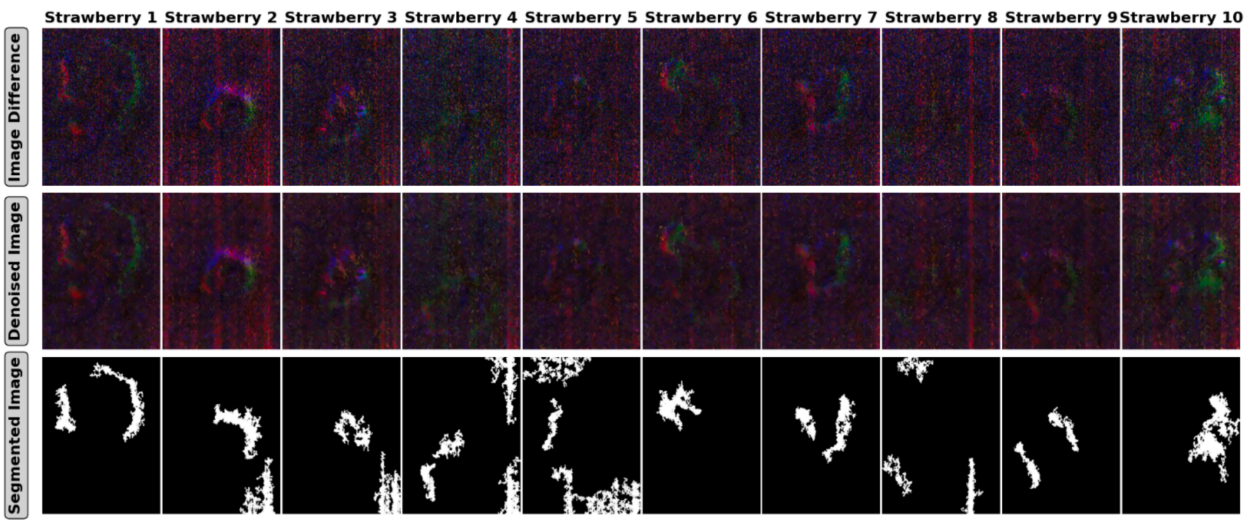

Fig. 21. Optical tactile sensing analysis of strawberries: Image processing workflow for strawberries 1 to 10 at 4 mm gripper width differences.

scattered pixel variations suggests additional processing is necessary to enhance feature clarity. The second row, Denoised Image**,** shows the results after applying a noise-reduction technique. This process improves the visibility of features by suppressing background noise while preserving the primary structural details of the strawberries. The denoised images represent the key regions of interest, making subsequent segmentation more reliable. The third row, Segmented Image, represents where key areas are extracted based on predefined segmentation criteria. The white regions indicate detected features, while the black regions denote background areas.

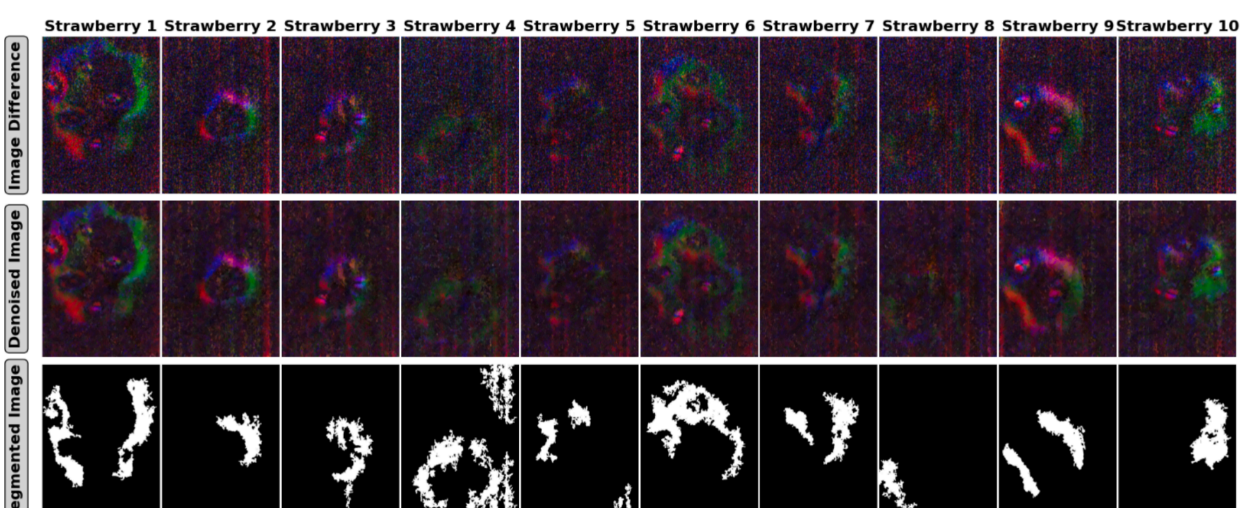

Fig. 22. Optical tactile sensing analysis of strawberries: Image processing workflow for strawberries 1 to 10 at 8 mm gripper width differences.

Strawberries 1 to 10 exhibited successful segmentation, as shown in Fig. 21, indicating the framework's robustness across various specimens. Nonetheless, minor noise issues were observed in Strawberry 2, 3, 4, and 5, likely due to their position at the beginning of the compression process. The overall performance underscores the efficacy of the proposed methodology in accurately delineating deformation areas induced by the DIGIT sensor.

In Fig. 22, the framework successfully segments most strawberries, demonstrating the system's robustness. However, minor artifacts are still noticeable in regions 4 and 5.

In Fig. 23, the segmentation process is successfully applied to all strawberries. As pressure increases, the segmentation results show reduced noise interference, particularly at a gripper width difference of 12 mm. A subtle difference between Figs. 21 and 22 can be observed in strawberries 1 and 6, due to the increased pressure on the strawberries, leading to slight variations in the results. This highlights the sensitivity of the segmentation process to gripper width. This consistency across segmentation outcomes between Figs. 21 and 22 reinforces the efficacy of the segmentation approach across varying conditions and highlights its robustness.

Additionally, notable extra deformation parts are observed on strawberries across all strawberries. This phenomenon is attributed to the strawberries' width differences, resulting in larger deformation areas. The gripper width, in this instance, is reduced by 12 mm. Compared to the 4 mm reduction discussed previously, the area of interest has grown, indicating an increased compression effect. The correlation between the reduced width of the gripper and the deformation size underscores the sensitivity of the segmentation process to variations in the strawberry condition, offering valuable insights into the dynamic nature of deformation under different gripper widths. The experiments have demonstrated that the proposed method effectively captures the deformation effects of strawberries using the vision-based tactile sensor (VBTS). This capability aids in evaluating fruit grasping and can reduce damage during handling.

Fig. 24 illustrates the correlation between gripper width difference (mm) and segmented pixel area for 30 strawberry samples (s1 to s30), analysed through optical tactile sensing. The x-axis represents the gripper width difference, while the y-axis denotes the segmented pixel area obtained via image processing. Overall, an increasing trend in segmented pixel area with higher width differences is evident, indicating progressive deformation and enhanced sensor-surface contact. Strawberries 5,14,18,19,28, and 30, in particular, demonstrate fluctuations in segmentation performance, likely due to their unique morphological attributes and positioning relative to the DIGIT sensor. Variations in fruit shape, size, and internal structural composition contribute to these fluctuations, potentially impeding the framework's ability to consistently capture accurate deformation patterns for strawberries with more complex structures. Nevertheless, despite these inherent morphological and positional challenges, the overall positive trend suggests that the optical tactile sensing framework effectively characterizes deformation patterns in strawberries.

4.3.2. Blueberry case example

Following the testing on strawberries, blueberries were analysed next. Blueberries 1 to 10 demonstrated successful segmentation, as illustrated in Fig. 25, highlighting the framework's robustness across different specimens. Minor noise artifacts were observed in blueberries 5 through 10, likely caused by their structural characteristics. Despite these slight inconsistencies, the overall results reinforce the effectiveness of the proposed methodology in accurately capturing deformation patterns induced by the DIGIT sensor.

In Fig. 26, the system effectively segments the majority of the blueberries. The minor noise represented in 3 and 9 was eliminated, except for blueberries 5, 8, and 10, which retain noise due to highly noisy artifacts present in the image.

In Fig. 27, the segmentation process is successfully applied to all blueberries, demonstrating its consistency across varying pressure levels. As pressure increases, noise interference is notably reduced, particularly at a gripper width difference of 16 mm.

A subtle difference between Figs. 26 and 27 is noticeable for blueberries 1 and 2, due to the increased applied pressure, resulting in slight variations in the segmentation outcomes. This highlights the sensitivity of the segmentation process to minor changes in gripper width. Meanwhile, blueberries 10 continue to pose segmentation challenges, primarily due to their structural characteristics and positioning within the tactile sensor, underscoring the importance of consistent positioning for optimal segmentation accuracy.

Fig. 28 presents the relationship between the gripper's width difference (mm) and segmented pixel area across 30 blueberry samples (b1–b30). While a general trend suggests a slight positive correlation, indicating an increase in segmented pixel area as the width difference increases, this trend is not uniformly clear across all samples. Noticeable variability and fluctuations exist, with several samples displaying inconsistent trends, especially blueberries 6,8,14,15, 17,18, 23, and 29.

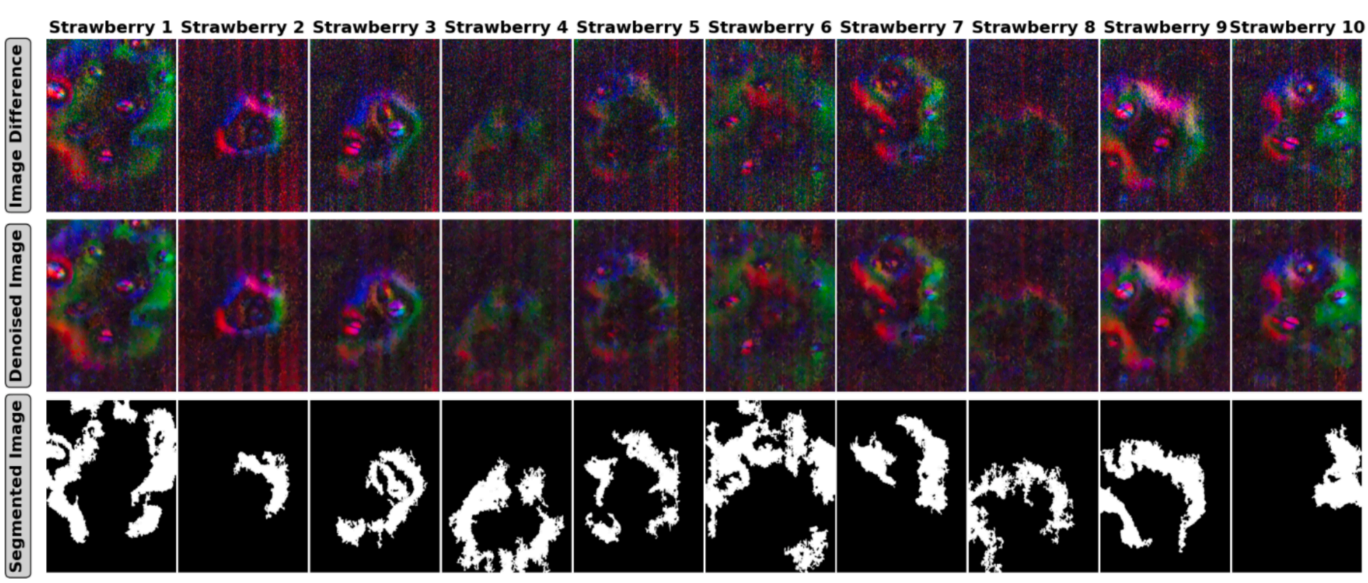

Fig. 23. Optical tactile sensing analysis of strawberries: Image processing workflow for strawberries 1 to 10 at 12 mm gripper width differences.

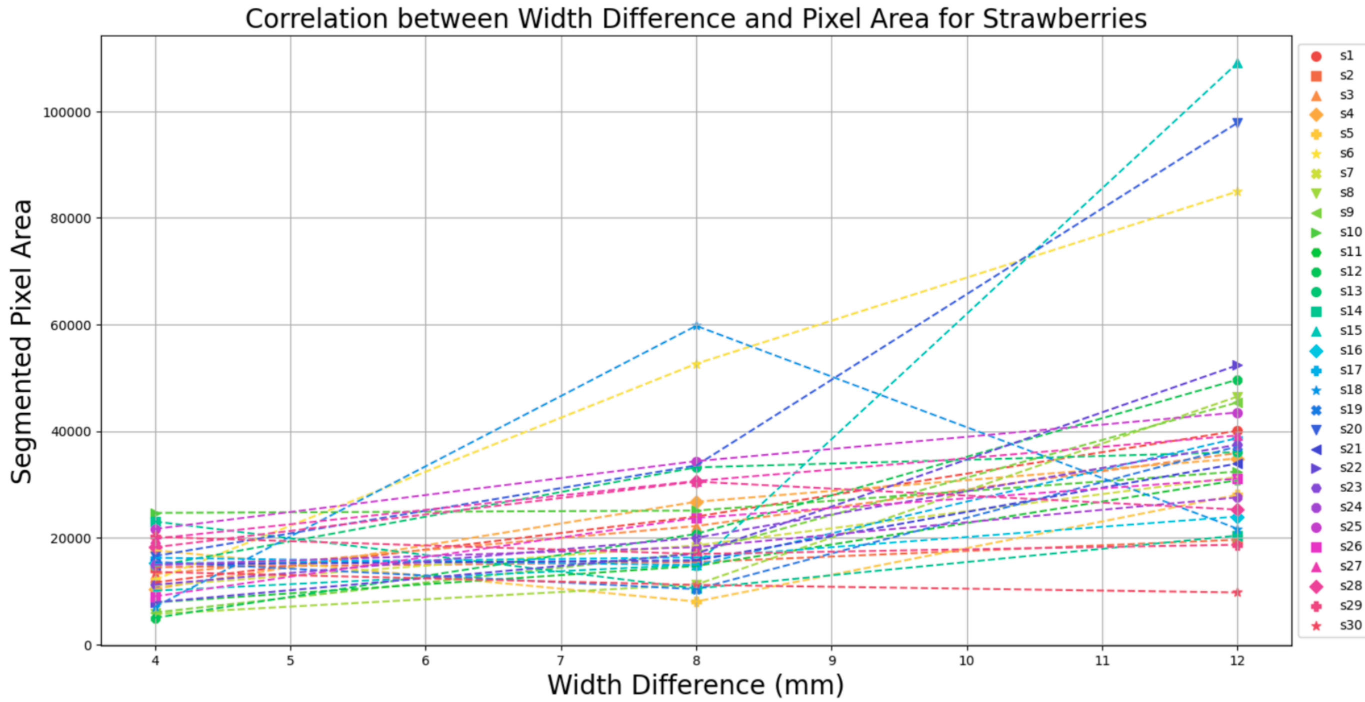

Fig. 24. Correlation between gripper width variation and segmented pixel area in optical tactile sensing of strawberries.

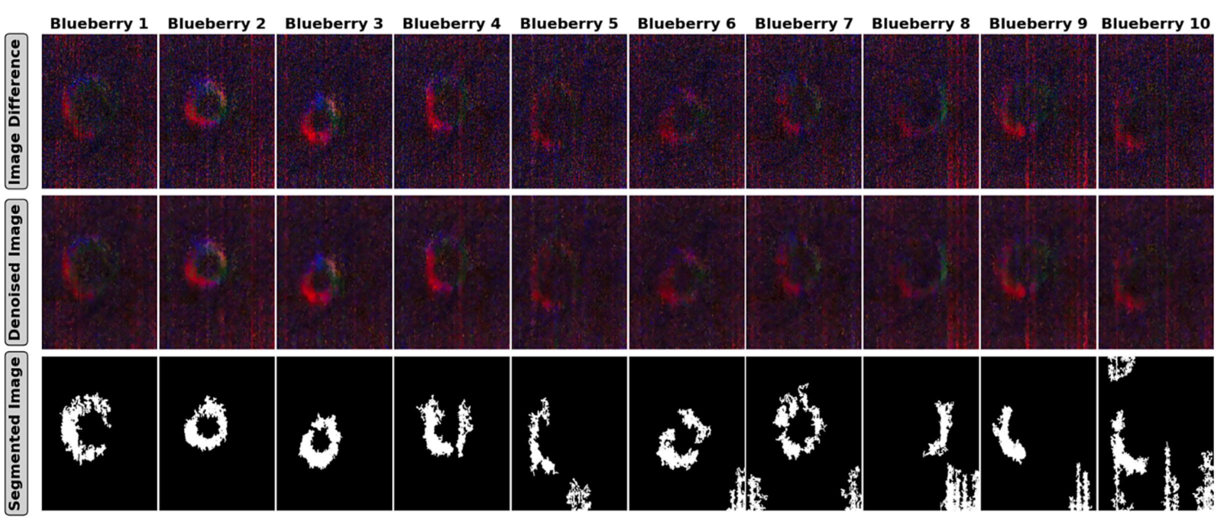

Fig. 25. Optical tactile sensing analysis of blueberries: Image processing workflow for blueberries 1 to 10 at 8 mm gripper width differences.

Such variations likely arise due to individual morphological characteristics, including shape, size, and positioning within the sensing system. Therefore, although the data implies that the optical tactile sensing framework can generally capture deformation patterns effectively, it also highlights certain limitations and inconsistencies when handling blueberries with subtle morphological differences or positioning variability.

4.3.3. Raspberry case example

Fig. 29 illustrates the segmentation surface deformations in raspberry samples. Raspberries 3, 5, 6, 7, 9, and 10 presented challenges, likely due to their complex morphology and structural inconsistencies. These particular raspberries' irregular texture and porous surface introduced additional difficulties for the opto-tactile sensor, thereby reducing segmentation accuracy. While raspberries 1, 2, and 4 were segmented effectively, the framework's performance was significantly affected by the raspberries' irregular morphology.

With a 12 mm gripper width difference (Fig. 30), segmentation accuracy improved due to enhanced contact between the gripper and the raspberry surface. While some raspberries were successfully segmented, Raspberries 2, 5, 8, 9, and 10 remained challenging. The increased pressure helped the sensor capture more detailed surface features, making deformation patterns more apparent in some samples.

Fig. 31 shows that segmentation was set at a 16 mm gripper width difference, with only raspberries 6, 7,9, and 10 failing to segment effectively. The increased compression further reduced noise interference, improving the delineation of surface deformations. However, challenges persist in accurately extracting the contact area of the raspberries.

The structural intricacies of raspberries, including their porous and uneven surface, present inherent challenges for segmentation, necessitating optimal compression levels to enhance image clarity and

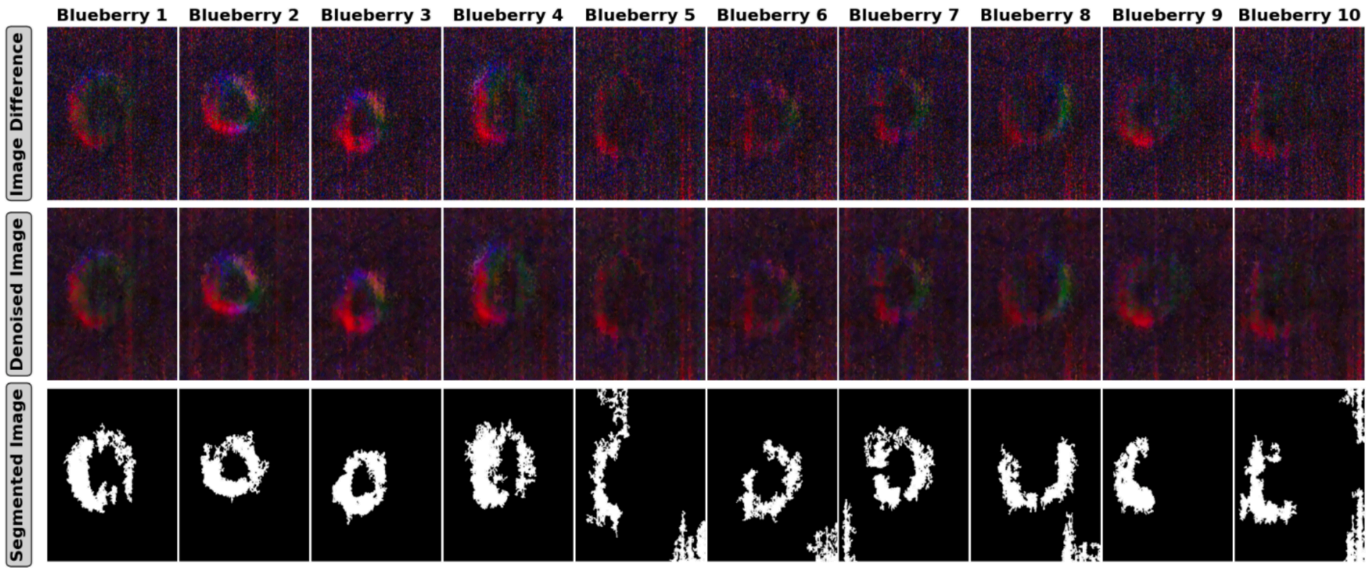

Fig. 26. Optical tactile sensing analysis of blueberries: Image processing workflow for blueberries 1 to 10 at 12 mm gripper width differences.

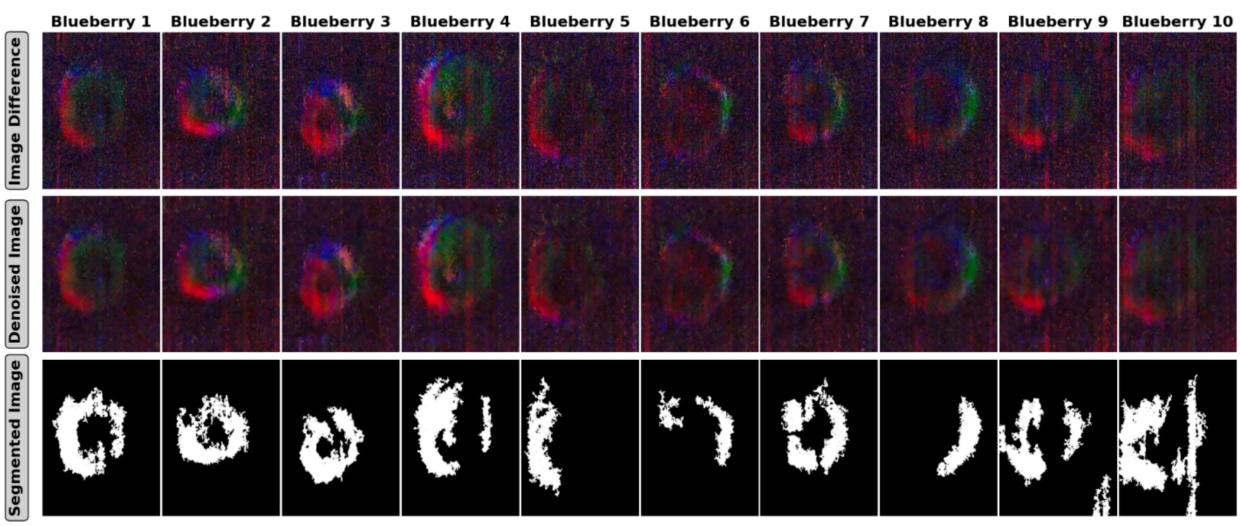

Fig. 27. Optical tactile sensing analysis of blueberries: Image processing workflow for blueberries 1 to 10 at 16 mm gripper width differences.

processing accuracy.

Fig. 32 illustrates the correlation between gripper width difference (mm) and segmented pixel area across 30 raspberry samples (r1 to r30). The data demonstrate considerable variability among samples. Although small number of raspberries exhibit relatively stable or gradually increasing segmented areas with increased gripper width differences, several samples, including r2, r3, r5, r9, r10, r12, r13, r14, r15, r17, r19, r21, r22, r24, r26, r27, r28, and r30, showed segmentation failures. These samples displayed pronounced fluctuations and inconsistencies in segmented area measurements, highlighting evident segmentation failures likely due to morphological irregularities, structural inconsistencies, and porous surface textures. These findings emphasize that, despite the framework's general effectiveness, critical challenges persist in reliably capturing deformation patterns in structurally complex raspberries.

Table 6 summarizes the segmentation failure rates observed during compression tests conducted on three types of soft fruits: strawberries, blueberries, and raspberries. For each fruit type, a total of 30 samples were analysed. The column labelled "Unexpected Samples" indicates the number of samples that exhibited segmentation failures, characterized by pronounced inconsistencies, fluctuations, or inaccuracies in segmented pixel area measurements during deformation. The percentage of unexpected samples highlights the relative frequency of segmentation failures, demonstrating that raspberries experienced the highest failure rate (60.0 %), significantly greater than strawberries (20.0 %) and blueberries (26.7 %). This underscores the challenges associated with accurately quantifying deformation in fruits possessing more complex morphological structures and irregular surface textures, such as raspberries.

4.4. Sensitivity of the image processing pipeline

The image processing pipeline demonstrated varying degrees of sensitivity depending on the gripper width during strawberry compression. Figs. 21-23 show that the pipeline successfully segmented the deformed regions with increasing precision as the gripper width was reduced. A similar trend was observed in blueberries (Figs. 25–27) and raspberries (Figs. 29–31), where increased compression improved segmentation by enhancing sensor contact with the fruit surface. The segmentation quality improved with each incremental step, as indicated by the progressively larger deformation areas detected. These results suggest that the pipeline is sensitive to subtle changes in surface

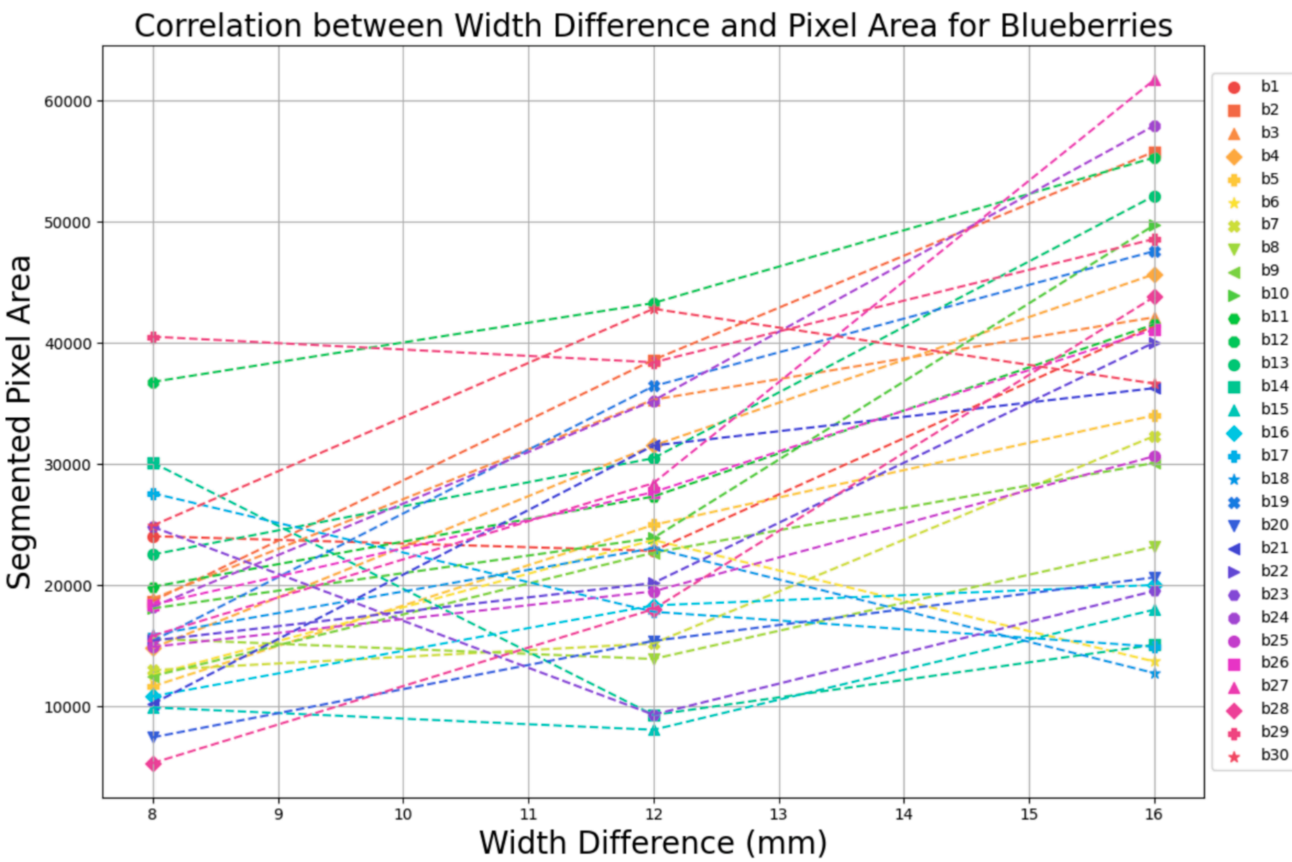

Fig. 28. Correlation between gripper width variation and segmented pixel area in optical tactile sensing of blueberries.

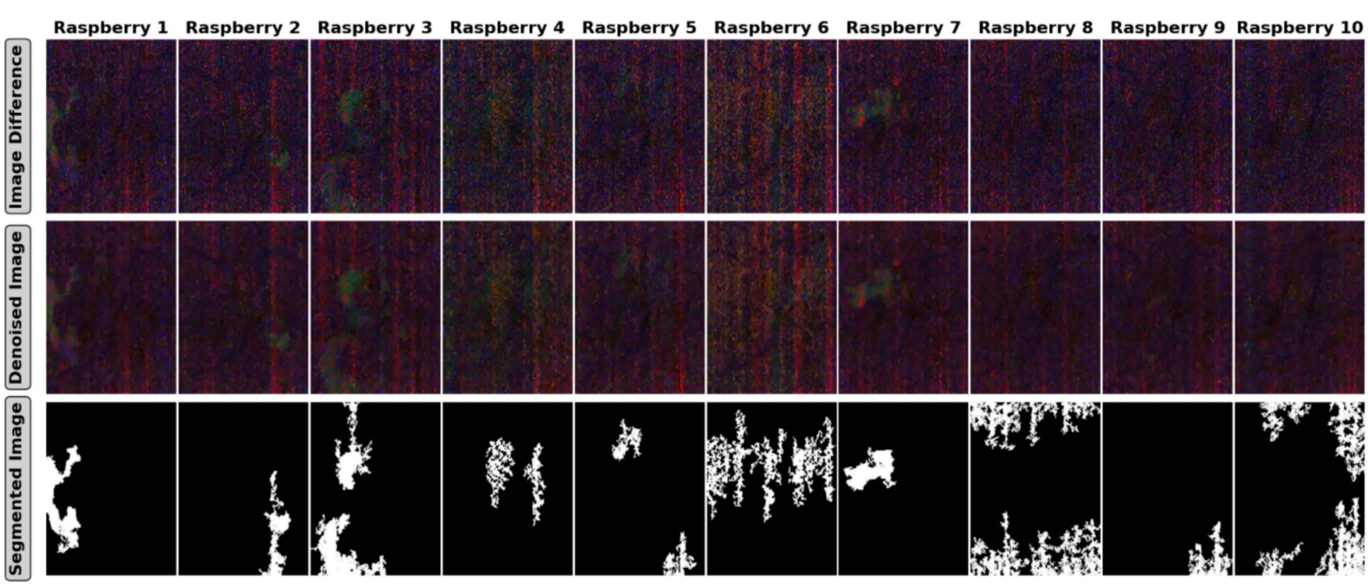

Fig. 29. Optical tactile sensing analysis of raspberries: Image processing workflow for raspberries 1 to 10 at 8 mm gripper width differences.

morphology, especially when dealing with materials exhibiting non-linear deformation characteristics. Furthermore, as observed in the histogram analysis of the RGB channels (Figs. 6-8), small shifts in intensity were detected even at lower gripper widths, suggesting that the pipeline can capture surface texture changes well. This sensitivity is particularly pronounced when comparing the results of the rubber ball and soft fruits, where more complex deformation patterns were still detected at a high sensitivity level. The results indicate that the pipeline is susceptible to changes in surface morphology, even at minimal compression levels. The gradual reduction in gripper width allowed for precise deformation detection, showcasing the system's ability to differentiate between subtle changes in the surface of strawberries, blueberries, and raspberries. This sensitivity is essential for applications where accurate handling of delicate objects is required, as it ensures that the robotic system can detect and respond to minor variations in material properties.

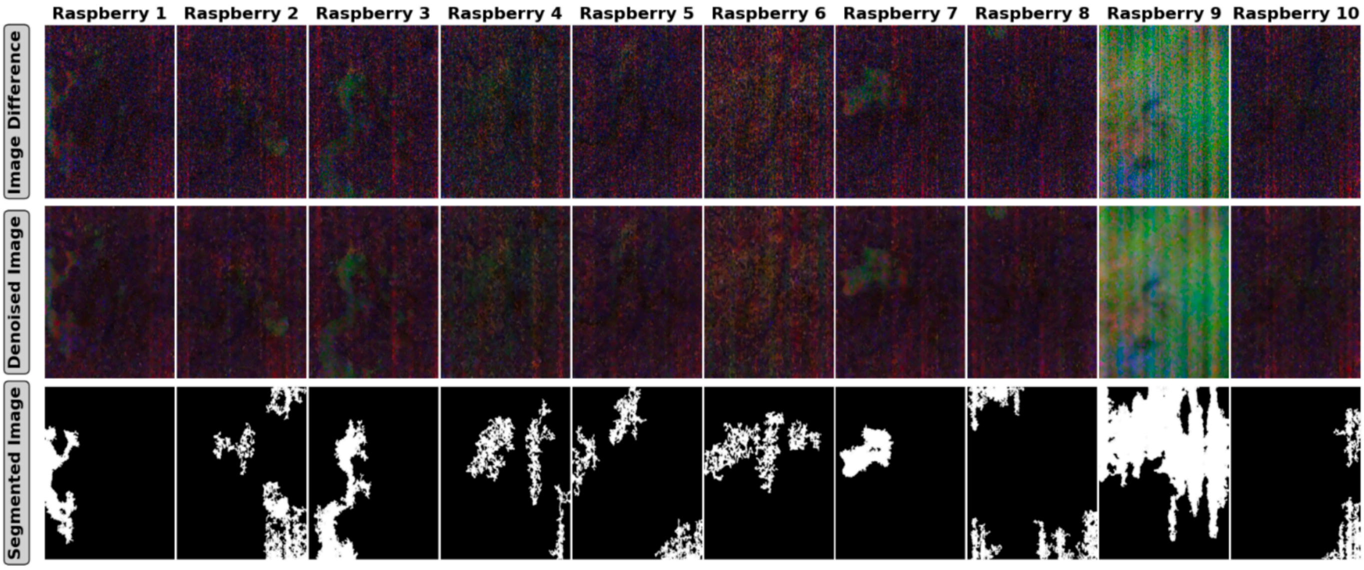

Fig. 30. Optical tactile sensing analysis of raspberries: Image processing workflow for raspberries 1 to 10 at 12 mm gripper width differences.

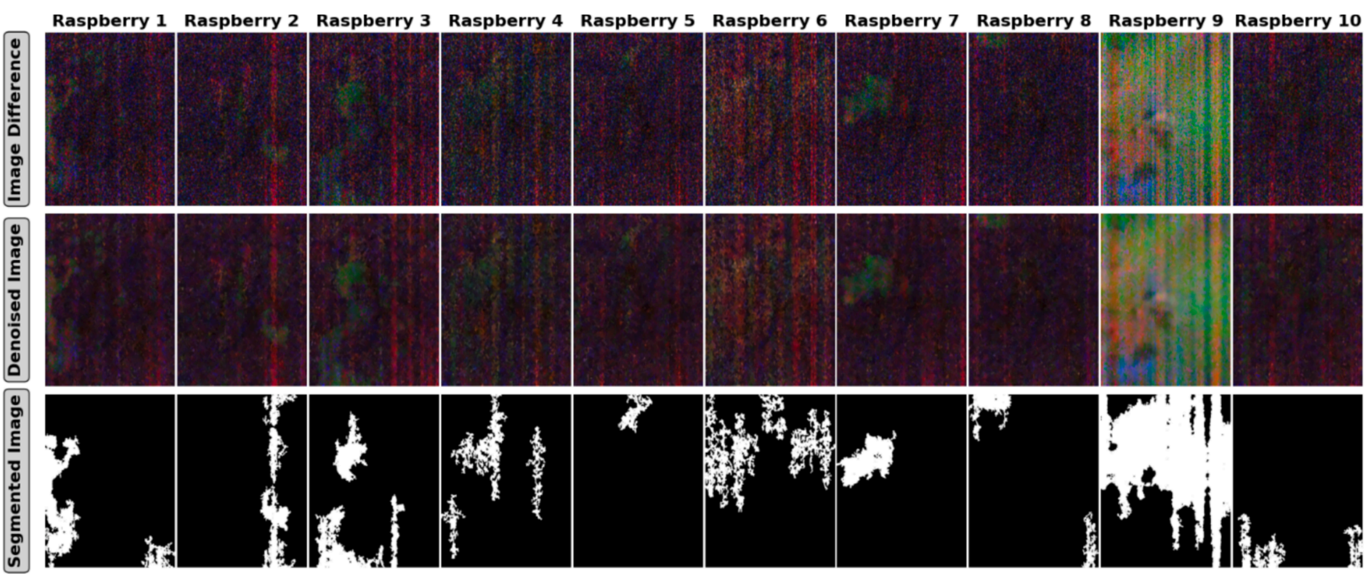

Fig. 31. Optical tactile sensing analysis of raspberries: Image processing workflow for raspberries 1 to 10 at 16 mm gripper width differences.

5. Discussion

Addressing the research question posed above, this study offers distinct insights into integrating vision-based tactile sensors in assessing delicate objects like soft fruits, with a case example using strawberries, blueberries, and raspberries. The efficacy of advanced image processing techniques to accurately quantify deformation in strawberries using vision-based tactile sensors was explored. The image processing pipeline's ability to measure deformation is crucial for handling soft fruits because it allows the robotic system to understand how the fruit's surface changes under pressure. By accurately measuring deformation, the system can adjust its grip to apply just the right amount of pressure, enough to securely hold the fruit without causing damage. This ensures that the fruit is handled gently and precisely, reducing the risk of bruising or crushing, which is particularly important for soft and delicate fruit.

Compared with existing studies, our approach offers a novel perspective on analysing deformation in soft fruit, particularly strawberries, using advanced image processing techniques combined with tactile sensing. For instance, Shah et al. (2021) demonstrated high classification accuracy for predicting the firmness of tomatoes and nectarines using a CNN-LSTM model. Their approach primarily focused on leveraging deep learning for classification tasks, effectively capturing firmness characteristics. He et al. (2024) assessed peach firmness using a visuo-tactile sensor integrated with a CNN-LSTM architecture, achieving an R^2 value of 0.88 and RMSE of 0.719. Their study emphasised optimising image sequence length and preprocessing techniques to enhance model performance. While these studies provided valuable insights into fruit firmness prediction, our methodology diverges by focusing on quantifying deformation in soft fruits like strawberries, blueberries, and raspberries through opto-tactile data. Similarly, Li et al. (2024) developed a deep learning framework for fruit hardness estimation using the DIGIT sensor, employing a Capsule Network with a self-attention mechanism to regress hardness values from tactile images. In contrast, our approach leverages an image-processing pipeline that emphasises localised surface deformations through difference imaging, unsupervised clustering, and morphological analysis. Unlike the methods that rely heavily on deep learning architectures, our approach integrates

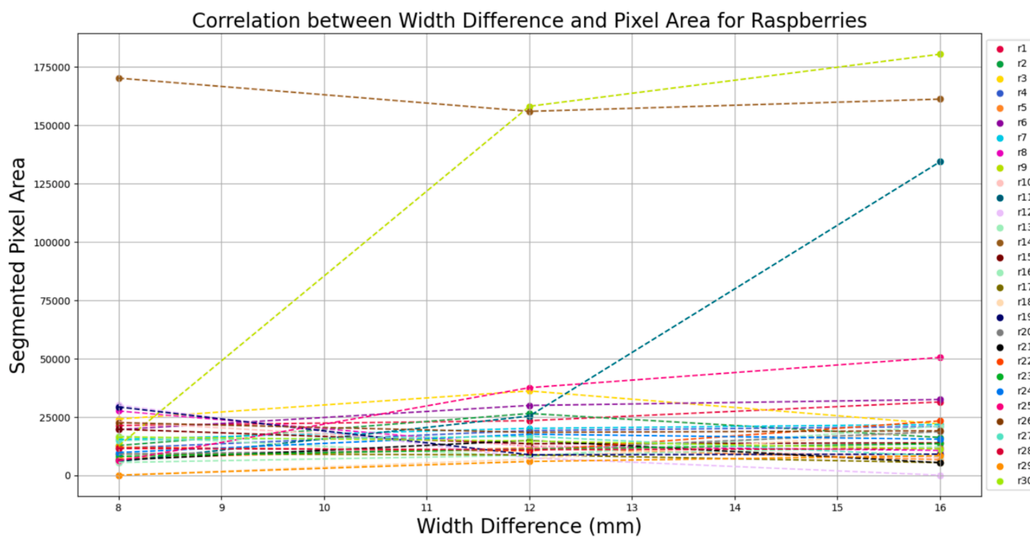

Fig. 32. Correlation between gripper width variation and segmented pixel area in optical tactile sensing of raspberries.

Table 6
Summary of segmentation failures across fruit types.

Fruit Type	Total samples	Unexpected Samples	Percentage Unexpected
Strawberry	30	6	20.0 %
Blueberry	30	8	26.7 %
Raspberry	30	18	60.0 %

advanced image processing techniques, including denoising, K-means clustering, morphological operations, and connected components analysis, all processed through the DIGIT sensor. This system allows for a detailed analysis of surface deformations, capturing subtle changes that occur during the handling process. The approach proposed and tested in this paper offers several distinct advantages. We can highlight minor deformations that may go unnoticed in standard analysis by employing image differencing and amplification. Combining denoising with K-means clustering and morphological operations further refines the segmentation process, ensuring that even the most delicate surface changes are accurately captured. Moreover, we demonstrate the method's sensitivity to varying compression levels by analysing the correlation between gripper width and deformation size, as observed in the difference between smaller and larger gripper widths. This capability is crucial for applications in automated harvesting, where precise control over grip strength and deformation is necessary to prevent damage to delicate produce. Furthermore, our method addresses the challenge of accurately measuring deformation without relying on direct force measurements. This is particularly important in scenarios where direct measurement may be impractical or potentially damage the fruit. By focusing on minor deformation patterns, our approach can be adapted to handle various fruit types, accommodating differences in size, shape, and ripeness. This adaptability enhances the versatility of robotic systems in agricultural settings. In contrast to the works by Zhou et al. (2023) and Yamaguchi & Atkeson (2019), which employed tactile sensor arrays and FingerVision® technology to enhance robotic grasping and handling capabilities, our method prioritises the detailed analysis of deformation patterns. While those studies focused on enhancing robotic perception and manipulation of diverse objects, our approach contributes to understanding how soft fruits deform under varying grip conditions. This knowledge can inform the development of more sophisticated robotic systems capable of gentle and precise manipulation.

With its predictable deformation behaviour, the rubber ball provided a controlled environment for calibrating the software pipeline. The pipeline effectively captured and analysed the surface deformations of the rubber ball, given its uniform elasticity and response to compression. While the advantages of the proposed and tested novel opto-tactile sensing approach to enhance the handling of soft fruit were demonstrated by the results obtained from the rubber ball, further work might test how results might rely on linear and consistent material properties. Further testing applied to soft materials or non-linear organic substances, which exhibit highly nonlinear and unpredictable deformation characteristics, can follow.

The analysis began with varying gripper width differences tailored specifically for each fruit type: strawberries (4 mm), blueberries (8 mm), and raspberries (8 mm). These initial conditions marked the thresholds at which the segmentation pipeline successfully delineated deformation areas captured by the DIGIT sensor. Before reaching these thresholds, accurate segmentation was limited due to insufficient compression and elevated noise levels, obscuring precise identification of deformation regions. For strawberries (Figs. 21-23), starting at a 4 mm gripper width difference significantly improved segmentation clarity, distinctly identifying deformation areas. As the gripper width increased to 8 mm and subsequently 12 mm, segmentation accuracy progressively improved, with deformation regions becoming more pronounced, reflecting a clear correlation between applied pressure and segmentation quality.

A comparable trend was observed with blueberries (Figs. 25-27), where successful segmentation began at 8 mm, establishing an initial foundation. Although segmentation was achieved at this stage, noticeable noise obstructed the clarity, making it difficult to achieve accurate results. Improvements were observed at 12 mm and further at 16 mm gripper width differences. This demonstrates the effective adaptability of the denoising and clustering techniques in capturing deformation characteristics of smaller, more rigid fruits under increased compression. With their porous and irregular morphologies, raspberries (Figs. 29-31) initially exhibited successful segmentation at a gripper width difference of 8 mm. Subsequent incremental increases to 12 mm and 16 mm notably enhanced segmentation accuracy, reducing noise interference and clarifying deformation areas. However, the structural complexities inherent in raspberries continued to present segmentation challenges despite increased compression. Nonetheless, the overall positive correlation between gripper width differences and segmentation performance underscores the flexibility and effectiveness of the proposed methodology. It should be noted that employing a fixed number of clusters in the K-means algorithm remains a potential limitation, as it may not fully accommodate the morphological diversity and varying deformation patterns observed among different fruit samples.

6. Limitations of the current study

Although this study demonstrates that a vision-based tactile sensor (VBTS) can effectively measure surface deformation in strawberries, raspberries, and blueberries, several avenues remain for future research to further enhance the accuracy and applicability of the proposed approach. First, the absence of a compression testing machine presents an opportunity for more rigorous validation: incorporating controlled mechanical tests or standardised weight-based checks would allow researchers to correlate optical deformation measurements with absolute force–displacement data directly. While this study relied upon high-precision industrial hardware, the Robotiq 2F-85 gripper with a known gripping repeatability of $\pm$ 0.05 mm to provide a stable and controlled grasping baseline, including standard mechanical benchmarking, would further strengthen validation. Second, while the pipeline adeptly captured deformation in all three fruit types, challenges were notably higher for raspberries due to their porous and irregular morphology. Future work might explore advanced segmentation algorithms, hybrid sensing modalities (e.g., thermal or multispectral imaging), or adaptive machine learning models that account for different fruits' nonlinear elasticity and heterogeneous structures. Third, expanding the pipeline to a broader range of fruits or agricultural products combined with finite element simulations could further elucidate how diverse shapes, sizes, and internal textures influence sensor readings and segmentation outcomes. Finally, integrating real-time feedback loops into robotic handling systems would enable dynamic grip width adjustments, minimising damage while maintaining throughput in industrial harvest and post-harvest operations. By pursuing these directions, researchers can deepen the scientific understanding of tactile sensing and advance the practical deployment of VBTS technologies in precision agriculture.

7. Conclusions

We proposed and tested a novel opto-tactile sensing approach to enhance the handling of soft fruits. Our work introduces an automated deformation measurement pipeline leveraging vision-based tactile sensors, specifically validated with strawberries, raspberries, and blueberries. We extracted critical insights into fruit deformation characteristics using denoising techniques, machine learning, morphological operations, and connected component analysis. By focusing our validation efforts on a rubber ball as a benchmark object, this research demonstrates for the first time the practical application of this methodology and processing pipeline for precise deformation measurement, offering a promising foundation for improved fruit quality assessment in agricultural contexts. Although challenges such as residual image noise were encountered, our findings establish the viability of vision-based tactile sensing systems in supporting more informed decision-making and enhancing overall handling performance. Future research could extend this pipeline by integrating real-time adaptive grip force control to optimize robotic handling strategies further, minimizing damage and maximizing efficiency in commercial agricultural operations.

CRediT authorship contribution statement

Mohamed Adlan Ait Ameur: Writing – review & editing, Writing – original draft, Visualization, Validation, Software, Methodology, Investigation, Formal analysis, Data curation, Conceptualization. **Amr M. El-Sayed:** Writing – review & editing, Visualization, Validation, Methodology, Investigation, Formal analysis, Conceptualization. **Xiu T. Yan:** Writing – review & editing, Supervision, Funding acquisition. **Jörn Mehnen:** Writing – review & editing, Supervision, Resources, Project administration, Funding acquisition. **Anja M. Maier:** Writing – review & editing, Supervision, Project administration, Resources, Funding acquisition.

Declaration of competing interest

The authors declare that they have no known competing financial interests or personal relationships that could have appeared to influence the work reported in this paper.

Acknowledgement

We acknowledge support from the Made Smarter Innovation - Research Centre for Smart, Collaborative Industrial Robotics with grant ID EP/V062158/1 and the Department of Design, Manufacturing and Engineering Management (DMEM) at the University of Strathclyde in Glasgow, United Kingdom.

Data availability

DOI not available yet.

References

Bechar, A., Vigneault, C., 2016. Agricultural robots for field operations: concepts and components. Biosyst. Eng. 149, 94–111.
Benos, L., Moysiadis, V., Kateris, D., Tagarakis, A.C., Busato, P., Pearson, S., Bochtis, D., 2023. Human–robot interaction in agriculture: a systematic review. Sensors 23 (15), 6776.
Buades, A., Coll, B., Morel, J.-M., 2011. Non-local means denoising. Image Process. Line 1, 208–212.
Chen, Y., Lin, J., Du, X., Fang, B., Sun, F., & Li, S. (2022). Non-destructive fruit firmness evaluation using vision-based tactile information. 2022 International Conference on Robotics and Automation (ICRA).
Comer, M.L., Delp III, E.J., 1999. Morphological operations for color image processing. J. Electron. Imaging 8 (3), 279–289.
Datacarpentry. (2024). *Image Processing with Python: Connected Component Analysis.* Retrieved 05 Feb from https://datacarpentry.org/image- processing/08-connected-components.html.
De Maria, G., Natale, C., Pirozzi, S., 2012. Force/tactile sensor for robotic applications. Sens. Actuators A: Phys. 175, 60–72.
Duckett, T., Pearson, S., Blackmore, S., Grieve, B., Chen, W.-H., Cielniak, G., Cleaversmith, J., Dai, J., Davis, S., & Fox, C. (2018). Agricultural robotics: the future of robotic agriculture. *arXiv preprint arXiv:1806.06762*.
Fahmy, I., Hassan, T., Hussain, I., Seneviratne, L., Werghi, N., 2024. Vision- based tactile sensors in precision agriculture: deep learning approaches. Applications and Limitations.
United Nations (2019). *World Population Prospects 2019: Highlights*, New York, ST/ESA/SER.A/423, ISBN: 978-92-1-148316-1.
Girão, P.S., Ramos, P.M.P., Postolache, O., Pereira, J.M.D., 2013. Tactile sensors for robotic applications. Measurement 46 (3), 1257–1271.
Han, Y., Yu, K., Batra, R., Boyd, N., Mehta, C., Zhao, T., She, Y., Hutchinson, S., & Zhao, Y. (2021). Learning generalizable vision-tactile robotic grasping strategy for deformable objects via transformer. *arXiv preprint arXiv:2112.06374*.
He, L., Tao, L., Ma, Z., Du, X., Wan, W., 2024. Cherry tomato firmness detection and prediction using a vision-based tactile sensor. J. Food Measure. Character. 18 (2), 1053–1064.
Kakani, V., Cui, X., Ma, M., Kim, H., 2021. Vision-based tactile sensor mechanism for the estimation of contact position and force distribution using deep learning. Sensors 21 (5), 1920.
Ko, B.C., Nam, J.-Y., 2006. Object-of-interest image segmentation based on human attention and semantic region clustering. JOSA A 23 (10), 2462–2470.
Kodinariya, T.M., Makwana, P.R., 2013. Review on determining number of Cluster in K-Means Clustering. Int. J. 1 (6), 90–95.
Kootstra, G., Wang, X., Blok, P.M., Hemming, J., Van Henten, E., 2021. Selective harvesting robotics: current research, trends, and future directions. Curr. Robot. Rep. 2, 95–104.
Lambeta, M., Chou, P.-W., Tian, S., Yang, B., Maloon, B., Most, V.R., Stroud, D., Santos, R., Byagowi, A., Kammerer, G., 2020. DIGIT: a novel design for a low-cost compact high-resolution tactile sensor with application to in-hand manipulation. IEEE Rob. Autom. Lett. 5 (3), 3838–3845.
Li, S., Sun, W., Liang, Q., Liu, C., Liu, J., 2024. Assessing fruit hardness in robot hands using electric gripper actuators with tactile sensors. Sens. Actuators, A 365, 114843.
Lin, C., Lin, Z., Wang, S., & Xu, H. (2023). Dtact: A vision-based tactile sensor that measures high-resolution 3d geometry directly from darkness. 2023 IEEE International Conference on Robotics and Automation (ICRA).
Lin, J., Hu, Q., Xia, J., Zhao, L., Du, X., Li, S., Chen, Y., Wang, X., 2023b. Non-destructive fruit firmness evaluation using a soft gripper and vision- based tactile sensing. Comput. Electron. Agric. 214, 108256.
Mandil, W., Rajendran, V., Nazari, K., Ghalamzan-Esfahani, A., 2023. Tactile- sensing technologies: trends, challenges and outlook in agri-food manipulation. Sensors 23 (17), 7362.

Naeini, F.B., AlAli, A.M., Al-Husari, R., Rigi, A., Al-Sharman, M.K., Makris, D., Zweiri, Y., 2019. A novel dynamic-vision-based approach for tactile sensing applications. IEEE Trans. Instrum. Meas. 69 (5), 1881–1893.

OMNIVISION. OVM7692-RAAA. Retrieved 08 Feb from https://www.ovt.com/products/ovm7692-raaa/.

Robotiq. (2018). Robotiq 2F-85 & 2F-140 for e-Series Universal Robots. Retrieved 09 Feb from https://assets.robotiq.com/website- assets/support_documents/document/2F-85_2F- 140_Instruction_Manual_e-Series_PDF_20190206.pdf.

Shah, U.H., Muthusamy, R., Gan, D., Zweiri, Y., Seneviratne, L., 2021. On the design and development of vision-based tactile sensors. J. Intell. Rob. Syst. 102, 1–27.

UR10e. (2023). Technical Specifications Contact. Retrieved 09 Feb from https://www.universal-robots.com/media/1807466/ur10e-rgb-fact- sheet-landscape-a4-125-kg.pdf.

Vasconez, J.P., Kantor, G.A., Cheein, F.A.A., 2019. Human–robot interaction in agriculture: a survey and current challenges. Biosyst. Eng. 179, 35–48.

Yamaguchi, A., Atkeson, C.G., 2019. Tactile behaviors with the vision-based tactile sensor FingerVision. Int. J. Humanoid Rob. 16 (03), 1940002.

Yuan, W., Dong, S., Adelson, E.H., 2017. Gelsight: high-resolution robot tactile sensors for estimating geometry and force. Sensors 17 (12), 2762.

Zhang, B., Xie, Y., Zhou, J., Wang, K., Zhang, Z., 2020. State-of-the-art robotic grippers, grasping and control strategies, as well as their applications in agricultural robots: a review. Comput. Electron. Agric. 177, 105694.

Zhang, S., Chen, Z., Gao, Y., Wan, W., Shan, J., Xue, H., Sun, F., Yang, Y., Fang, B., 2022. Hardware technology of vision-based tactile sensor: a review. IEEE Sens. J. 22 (22), 21410–21427.

Zhou, H., Kang, H., Wang, X., Au, W., Wang, M.Y., Chen, C., 2023. Branch interference sensing and handling by tactile enabled robotic apple harvesting. Agronomy 13 (2), 503.

Zou, L., Ge, C., Wang, Z.J., Cretu, E., Li, X., 2017. Novel tactile sensor technology and smart tactile sensing systems: a review. Sensors 17 (11), 2653.

Erukainure, F.E., Parque, V., Hassan, M.A., FathEl-Bab, A.M., 2022a. Design and experimental testing of a tactile sensor for self-compensation of contact error in soft tissue stiffness measurement. J. Mech. Sci. Technol. 36 (10), 5309–5324.

Erukainure, F.E., Parque, V., Hassan, M.A., FathEl-Bab, A.M., 2022b. Estimating the stiffness of kiwifruit based on the fusion of instantaneous tactile sensor data and machine learning schemes. Comput. Electron. Agric. 201, 107289.